

Showcasing research from the group of Professor Wonyong Choi at Pohang University of Science and Technology (POSTECH).

Photoinduced charge transfer processes in solar photocatalysis based on modified  $\text{TiO}_2$

Photocatalysis is being actively investigated as a core technology in solar light harvesting and utilizing processes. The basic process is driven by the photoinduced charge transfers (CTs) with initiating various redox reactions that are utilized for environmental remediation and solar energy storage. This Perspective article provides a comprehensive overview of the photoinduced CT events in bare and modified  $\text{TiO}_2$ , the most popular photocatalyst.

### As featured in:



See Wonyong Choi et al.,  
*Energy Environ. Sci.*, 2016, **9**, 411.



Cite this: *Energy Environ. Sci.*,  
2016, 9, 411

## Photoinduced charge transfer processes in solar photocatalysis based on modified TiO<sub>2</sub>

Hyunwoong Park,<sup>a</sup> Hyoung-il Kim,<sup>b</sup> Gun-hee Moon<sup>b</sup> and Wonyong Choi<sup>\*b</sup>

High efficiency solar photocatalysis requires an effective separation of photogenerated charge carriers and their rapid transport to the semiconductor interface. The mechanisms and kinetics of charge separation and interfacial/interparticle charge transfers (CT) are significantly influenced by both the bulk and surface properties of the semiconductor. The surface properties are particularly important because the photocatalysis should be driven by the interfacial CT. The most popular and the most investigated semiconductor photocatalyst is based on bare and modified TiO<sub>2</sub>. This article highlights the interfacial and interparticle CTs under the bandgap excitation of TiO<sub>2</sub> particles, visible light-induced photochemical processes *via* either dye-sensitization or ligand-to-metal CTs at surface modified TiO<sub>2</sub> particles, and the applications of the photo-processes to pollutant degradation and simultaneous hydrogen production. While a variety of surface modification techniques using various nanomaterials and chemical reagents have been developed and tested so far, their effects are very diverse depending on the characteristics of the applied photocatalytic systems and even contradictory in some cases. Better understanding of how the modification influences the photoinduced CT events in semiconductors is required, particularly for designing hybrid photocatalysts with controlled CTs, which is sought-after for practical applications of photocatalysis.

Received 20th August 2015,  
Accepted 1st December 2015

DOI: 10.1039/c5ee02575c

[www.rsc.org/ees](http://www.rsc.org/ees)

### Broader context

Photocatalysis based on semiconductor materials is being actively investigated as a core technology in solar light harvesting and utilizing processes. The basic process is driven by the photoinduced charge transfers (CTs) occurring on the irradiated semiconductor surface with initiating various redox reactions that are utilized for environmental remediation and solar energy storage. The former reaction is usually initiated by a single electron transfer under aerated conditions to generate reactive oxygen species whereas the latter proceeds *via* two or more electron transfers in the absence of molecular oxygen. Most of the former reaction systems are thermochemically spontaneous ( $\Delta G^\circ < 0$ ) and lead to the mineralization of organic pollutants whereas the latter is an energy uphill process ( $\Delta G^\circ > 0$ ) and often needs co-catalysts to facilitate the multi-electron transfer processes. The mechanisms and kinetics of interfacial/interparticle CTs are influenced by the bulk and surface properties of semiconductor. While various surface modification techniques have been developed so far, their effects are very diverse and even contradictory in some cases. Better understanding of how the modification influences the photoinduced CT events in semiconductors is required, particularly for designing hybrid photocatalysts with controlled CTs, which is sought-after for practical applications of photocatalysis.

## 1. Introduction

Solar energy is the main driver of most biological and global environmental processes. In addition, the need of harvesting and utilizing sunlight as a renewable source of energy is continuously increasing. Solar photocatalysis based on semiconductor materials has been extensively studied over the past

four decades and is still being actively investigated as a core technology in solar light harvesting and solar conversion processes.<sup>1–11</sup> The basic process is driven by the photoinduced charge transfers occurring on the irradiated semiconductor surface with initiation of a variety of redox conversion reactions. Most of the semiconductor photocatalytic processes have been studied for the production of solar fuels (*e.g.*, H<sub>2</sub>) and for the environmental purification of contaminated water and air.<sup>2–9</sup> As the cost of fossil fuels and the demand for advanced environmental remediation technologies increase, the fundamental studies on photocatalysis<sup>12–16</sup> as well as its practical applications<sup>6,17</sup> have received growing attention.<sup>18</sup> A bibliographic database web-engine (Scopus) search finds over 7500 and 3500 publications

<sup>a</sup> School of Energy Engineering, Kyungpook National University, Daegu 702-701, Korea

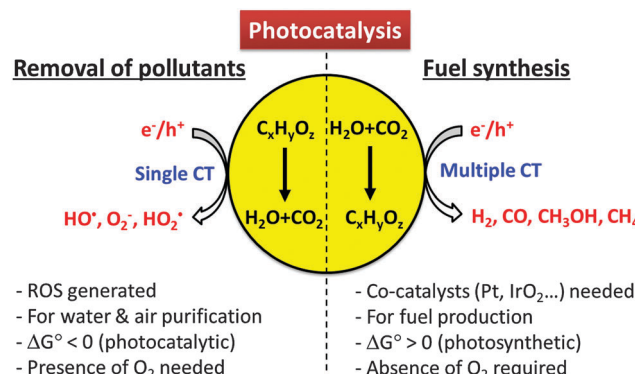
<sup>b</sup> School of Environmental Science and Engineering, Pohang University of Science and Technology (POSTECH), Pohang 790-784, Korea. E-mail: [wchoi@postech.edu](mailto:wchoi@postech.edu); Tel: +82-54-279-2283



in 2014 alone for the search keywords of photocatal\* and TiO<sub>2</sub>\* photocatal\*, respectively, which reflects the continued popularity of this research field.

A variety of semiconductor photocatalysts (TiO<sub>2</sub>,<sup>4,5,7,8,10,19</sup> ZnO,<sup>20–22</sup> WO<sub>3</sub>,<sup>23–27</sup> Fe<sub>2</sub>O<sub>3</sub>,<sup>28</sup> BiVO<sub>4</sub>,<sup>29–31</sup> CdS,<sup>25,32–34</sup> CdSe,<sup>35</sup> etc.) with different morphologies and modifications have been studied and developed. Photocatalysis is initiated by the light absorption by the semiconductor, followed by the charge-pair separation and interfacial charge transfer (CT). Since these reactions primarily occur on the surface, the modifications of semiconductor surface structures and properties significantly influence the overall photocatalytic reaction kinetics and mechanisms.<sup>7,8</sup> The imbalance of the interfacial CT of electrons and holes causes the charge pairs to rapidly recombine with each other, reducing or even nullifying the overall photocatalytic activity of interest. In this regard, proper understanding of the behavior of photogenerated CTs is necessary to achieve the desired reactions with high efficiency. With advancements in the fundamental studies on charge carrier dynamics,<sup>16</sup> the behaviors of photogenerated charge carriers have been more clearly elucidated. This helps us to understand how surface modification affects the photocatalytic processes in different ways, and eventually controls the photocatalytic pathways and activity.

The CT reactions occurring on semiconductor photocatalysts have been applied for two main purposes: (1) environmental applications for the remediation of polluted water and



Scheme 1 Comparison of photocatalytic reaction features for environmental purification *versus* solar fuel synthesis.

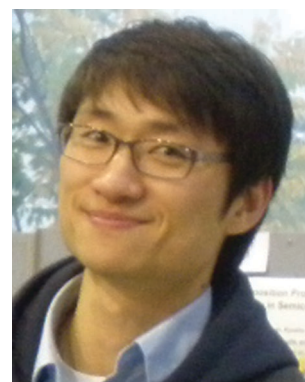
air and (2) solar energy storage through the synthesis of solar fuels (e.g., H<sub>2</sub> production from water splitting, CO<sub>2</sub> conversion to hydrocarbons). Scheme 1 illustrates how the characteristics of CTs in the two processes are different. The former process is usually initiated by a single electron transfer under aerated conditions to generate reactive radical species, whereas the latter proceeds *via* two or more electron transfers in the absence of molecular oxygen (O<sub>2</sub>). Generally, the photocatalytic degradation of organic compounds does not proceed in the absence of O<sub>2</sub>, whereas the photocatalytic production of solar fuels (e.g., H<sub>2</sub>, HCOOH) is very difficult to be achieved in the



Hyunwoong Park

Hyunwoong Park received a BS in Environmental Science at Hallym University in 1999 and a PhD degree (advisor: Wonyong Choi) in Environmental Engineering at POSTECH (Pohang, Korea) in 2004. After postdoctoral research at the California Institute of Technology (Pasadena, California: 2006–2008), he moved to the School of Energy Engineering at Kyungpook National University (Daegu, Korea) as an assistant professor (2008) and was then

promoted to associate professor (2012). He has published over 80 papers in peer-reviewed journals, which have been cited over 4500 times. He was awarded the Knowledge Creativity Award by the Ministry of Education, Science, and Technology, Korea (2012), and the Best Paper Award by the Korean Electrochemical Society (2013). He is serving as the Editor of Materials Science in Semiconductor Processing (Elsevier, since 2015) and the Associate Editor of Environmental Engineering Research (Korean Society of Environmental Engineers, since 2014). He is also on the editorial advisory boards of Journal of Environmental Chemical Engineering (Elsevier, since 2013) and International Journal of Photoenergy (Hindawi, since 2014).



Hyoung-il Kim

Hyoungil Kim received a BS in Environmental Engineering at Inha University (Incheon, Korea) in 2008 and a PhD degree (advisor: Wonyong Choi) in Environmental Engineering at POSTECH (Pohang, Korea) in 2014. He spent a half year at POSTECH as a postdoctoral researcher and is currently working in Chemical and Environmental Engineering at Yale University (New Haven, U.S.A.) as a postdoctoral researcher.



presence of O<sub>2</sub> because the molecular oxygen scavenges photo-generated electrons.<sup>36</sup> Most of the former reaction systems are thermochemically spontaneous ( $\Delta G^\circ < 0$ ) and lead to the mineralization of organic pollutants, whereas the latter for solar fuel synthesis is an energy uphill (energy-storing) process ( $\Delta G^\circ > 0$ ) and often needs co-catalysts (e.g., Pt,<sup>37</sup> Pd,<sup>38</sup> Co,<sup>29,39,40</sup> Ni,<sup>41,42</sup> Sn,<sup>43</sup> and Mn<sup>44</sup>) to facilitate the multi-electron transfer processes.

Some outstanding questions related to CT on semiconductor photocatalysts are as follows: (1) How can the recombination of charge pairs be minimized? (2) How can the single-electron transfer and the multi-electron transfer processes be controlled? (3) What determines the pathways of hole (or electron) transfer reactions leading to the generation of reactive radical species such as hydroxyl radical, superoxide, or singlet oxygen? Is it possible to control this selectively and if so, how? (4) How can visible light photons be utilized to induce CT in semiconductor photocatalysis? Such questions and the related research topics are listed as examples in Table 1. With these in mind, this article discusses the photoinduced CT occurring on semiconductor photocatalysts modified with various

methods developed by this research group and addresses the above questions.

## 2. Interfacial charge transfer

The interfacial CT characteristics required as a photocatalyst for environmental remediation and those as a photocatalyst for solar-fuel synthesis should be different. The former is mainly based on a single-electron transfer process, which accompanies the generation of reactive oxygen species (ROS) such as a hydroxyl radical and a superoxide (Fig. 1). On the other hand, the latter (solar fuel synthesis) proceeds through a multi-electron transfer process to synthesize energy-rich molecules (e.g., H<sub>2</sub>, CH<sub>3</sub>OH, CO, NH<sub>3</sub>) through the activation of thermochemically very stable precursors (e.g., H<sub>2</sub>O, CO<sub>2</sub>, N<sub>2</sub>). Under limited solar flux conditions, the transfer of multiple electrons and holes should be done through a sequential process of single electron transfer, which must involve various intermediate species. Since the intermediates are usually unstable and short-lived, the efficiency of multi-electron transfer is much lower than that



**Gun-hee Moon**

(2011–2012). He is currently working as a postdoctoral researcher in Prof. Choi's laboratory.

*Gun-hee Moon received a BS in Chemical Engineering at Inha University (Incheon, Korea) in 2008, an MS degree in Environmental Engineering from POSTECH in 2011, and a PhD degree (advisor: Wonyong Choi) in Chemical Engineering from POSTECH (Pohang, Korea) in 2015. He joined the Materials Science Division of Pacific Northwest National Laboratory (Richland, Washington) as an Alternate Sponsored Fellowship*



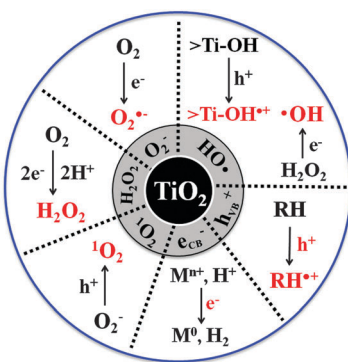
**Wonyong Choi**

*Wonyong Choi received a BS in engineering from Seoul National University (Seoul, Korea) in 1988, an MS in chemistry from POSTECH in 1990, and a PhD in chemistry from California Institute of Technology in 1996. After postdoctoral research in atmospheric chemistry at NASA/Caltech Jet Propulsion Laboratory (1996–1998), he joined the faculty of School of Environmental Science and Engineering, POSTECH as an assistant professor (1998), and was promoted to associate professor (2003), and full professor (2008). His research interests are mainly focused on semiconductor photocatalysis and photochemistry for solar energy conversion and environmental applications, advanced oxidation processes, and environmental chemistry. He has published over 230 papers in peer-reviewed journals, which have been cited over 23 000 times (H-index 60, Web of Science) to date. He received the Young Scientist Award (2006) and the KAST Science and Technology Award (2015) from the Korean Academy of Science and Technology (KAST), Lectureship Award from the Japanese Photochemistry Association (2008), Rising Star faculty fund from POSTECH (2011), Namgo chair professorship from POSTECH (2012) and was elected as Fellow of KAST and Fellow of Royal Society of Chemistry (FRSC) in 2014. Currently, he is serving as the Editor of Journal of Hazardous Materials (Elsevier, 2008–). He has been also on the editorial advisory boards of Energy and Environmental Science (RSC, 2008–), Environmental Science and Technology (ACS, 2015–), and Journal of Physical Chemistry (ACS, 2009–2011).*



Table 1 Some outstanding questions and the related topics on charge carrier behaviors in photocatalysis

Questions	Related topics	Research examples
How can the recombination of charge pairs be minimized?	Metal deposition Composites with carbon nanomaterials Doping (metals & non-metals) Electron shuttle Interparticle CT systems Heterojunctions (binary, tertiary, etc.)	23, 37, 98, 114, 241 33, 35, 145, 149, 242 28, 53, 54, 56, 57, 243–245 37, 85, 95 160–163, 166 25, 26, 32
How can multi-electron transfer processes be facilitated?	Catalysts for hydrogen evolution Catalysts for oxygen evolution Catalysts for CO <sub>2</sub> conversion Catalysts for H <sub>2</sub> O <sub>2</sub> production	33, 35, 80, 98, 145, 149, 246, 247 20, 28, 29, 45 139, 154, 248 82, 249
What influences the charge transfer reactions that lead to the generation of reactive oxygen species? Is it possible to control this selectively?	Fluorination Phosphonation Ion exchange resin Surfactants Polymers Structural engineering (porosity, surface area, nanostructure, etc.)	75, 77, 79, 80, 250 76, 80 61, 154, 215 223, 251 72, 211 163, 164, 166, 252
How can visible light photons be utilized to induce CT in photocatalytic systems?	Doping Dye sensitization Ligand-to-metal charge transfer (LMCT)	53, 54, 56, 57, 243–245 97, 98, 104, 166, 201, 207, 213–217 204, 205, 211

Fig. 1 Primary reactive oxygen species (ROS) generated in TiO<sub>2</sub> photocatalysis.

of the single-electron transfer process.<sup>45</sup> Since the CT characteristics are very different depending on the application purposes, a photocatalyst that is good for the degradation of organic pollutants can be poor for the solar fuel production if the single electron transfer is predominantly favored with a specific photocatalyst. The same can be said for the reverse case. The photochemical generation of ROS and the multi-electron transfer processes for fuel synthesis are vitally important in determining the photocatalytic activity but the detailed understanding of this critical process at the molecular level is still far from complete and the methods to control the CT behavior are limited.

Incidentally, considering that the earth crust is mainly composed of metal oxides including potentially photoactive ingredients like iron oxides, it is interesting to note that the lack of significant photoactivity in them under solar irradiation seems to be desirable to make the earth environment habitable for life. The efficient generation of ROS on solar irradiated metal oxides (soils and rocks) would have destroyed organic matters and microorganisms. If water splitting had occurred on

sunlit metal oxides, it might have changed the atmospheric composition that would be different from the current one (*e.g.*, elevated H<sub>2</sub> concentration in the atmosphere).

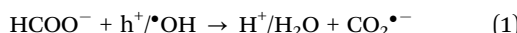
## 2.1. Charge transfers and the accompanying production of reactive species

**2.1.1. Valence band (VB) holes.** The irradiation of semiconductors excites electrons from the VB to the conduction band (CB) with leaving a hole (h<sup>+</sup>) in the VB and the oxidizing power of the hole often destabilizes the semiconductor material itself, which limits the practical applications of semiconductor photocatalysts. In this respect, TiO<sub>2</sub> is an excellent material that exhibits good photocatalytic activity and long-term stability in a wide pH range under both dark and irradiation conditions.<sup>8</sup> A fraction of photogenerated holes surviving the rapid recombination process diffuse to the semiconductor surface where they can react with any electron-donating species, which is a main driving force of most photocatalytic oxidation (PCO) processes. The reaction of the holes depends on both their oxidizing potential and the availability of adsorbed substrates. The holes readily react with strongly adsorbing molecules such as formates and oxalates (*i.e.*, electron donors), whereas they are less reactive with weakly adsorbing molecules (*e.g.*, chlorinated ethanes and chlorophenols).<sup>46–51</sup> The hole oxidation potential is essentially equal to the VB edge potential and depends on the kind of semiconductors. Semiconductors with a wide bandgap usually have highly positive VB potentials and the VB edge of TiO<sub>2</sub> that lies around ~2.7 V (vs. NHE at pH 7) induces the generation of strongly oxidizing holes under UV irradiation. The VB positions of metal oxide semiconductors like TiO<sub>2</sub> are usually similar among themselves because the VB mainly consists of the O 2p orbital that is a common component of oxide materials.<sup>12,52</sup> However, TiO<sub>2</sub> is unique not only in its highly oxidizing VB hole but also in its excellent (photo)chemical stability, abundance,



low material cost, and non-toxicity, which distinguish itself from other oxide semiconductors.

The oxidation power of photogenerated holes can be modified when impurity dopants (*e.g.*, transition metal ions, N, and C) are introduced into the TiO<sub>2</sub> lattice to create extra energy levels within the forbidden bandgap. Owing to the less positive levels of the dopant energy states in comparison to the original VB edge, the oxidizing power of the holes trapped at the dopant sites is less energetic.<sup>53,54</sup> This is why the visible light photocatalytic activities of doped TiO<sub>2</sub> are often limited compared with those of UV/TiO<sub>2</sub>.<sup>55–58</sup> For example, nitrogen-doped TiO<sub>2</sub> failed to catalyze the oxidation of formate (HCOO<sup>−</sup>) (reaction (1)) under visible irradiation ( $\lambda > 400$  nm) although it can absorb visible light up to  $\sim 600$  nm.<sup>55</sup>



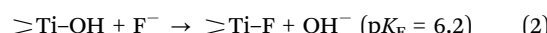
This was confirmed by the absence of the CO<sub>2</sub><sup>·−</sup> adduct with DMPO (5,5-dimethyl-1-pyrroline N-oxide) in the electron spin resonance spectra under visible light irradiation. Similar to this, the major oxidant in the photocatalysis of carbon-doped TiO<sub>2</sub> was suggested to be holes in the midgap states,<sup>57</sup> the potential of which is strong enough to directly oxidize 4-chlorophenol ( $E^\circ = 0.8$  V) but not enough to generate ·OH ( $E^\circ = 2.7$  V). Metal-doped TiO<sub>2</sub> samples exhibited the same phenomena. The photocatalytic degradation of tetramethylammonium (TMA: a probe substrate that can be degraded by ·OH radical) can be successfully achieved with bare TiO<sub>2</sub> under UV irradiation, whereas the visible activity of Pt<sub>ion</sub>-TiO<sub>2</sub> (Pt-doped) for the TMA degradation was negligible.<sup>56</sup> It is often regarded that the development of efficient visible light active photocatalysts is an ultimate goal in photocatalysis research but it should be realized that the available photocatalytic redox power under visible irradiation is sacrificed at the expense of utilizing lower energy photons, which limits the range of redox reactions that can be driven photocatalytically. The visible light photocatalysts are highly desired for solar conversion purposes but they are not a panacea.

**2.1.2. Hydroxyl radicals.** The most common hole trapping site on the metal oxide surface is the surface hydroxyl group and the hydroxyl radical is generated as a result of a hole reaction with a surface hydroxyl group or an adsorbed water molecule. The hydroxyl radical is one of the most powerful oxidants and reacts non-selectively with most organic substrates either *via* the abstraction of H atom (H<sup>·</sup>) from C-H bonds or *via* the addition to double bonds and aromatic rings. The resulting carbon-centered radical species (generated from the reaction with ·OH) subsequently combines with O<sub>2</sub> at a diffusion-limited rate to produce alkyl peroxy radicals which are eventually transformed into CO<sub>2</sub>. The ·OH-mediated PCO of refractory organic pollutants including polychlorinated dibenzo-*p*-dioxins (PCDDs),<sup>59,60</sup> TMA,<sup>23,56,61–63</sup> and carbon soot<sup>51,64</sup> are good examples demonstrating the superior oxidative power of OH radicals generated in the PCO process.<sup>50,59</sup>

The role of OH radicals in PCO processes is widely accepted and the photocatalytic degradation of pollutants on UV-illuminated TiO<sub>2</sub> through their action has been demonstrated for a large number of organic compounds. The OH radicals generated on

illuminated TiO<sub>2</sub> are present mainly in the form of surface bound hydroxyl radicals (·OH<sub>s</sub>).<sup>4,8</sup> However, it has been demonstrated that some fraction of OH radicals desorb from the surface as unbound radicals (free, ·OH<sub>f</sub>) and diffuse into the reaction medium. The previous studies investigated the desorption of ·OH<sub>f</sub> at the TiO<sub>2</sub>/air interface<sup>51,65–72</sup> and clearly demonstrated that the OH radicals generated from illuminated TiO<sub>2</sub> diffuse through the air to react with a substance that is not in direct contact with the TiO<sub>2</sub> surface. The diffusing radicals react with various remote substrates (*e.g.*, carbon soot,<sup>51,64,67,73</sup> stearic acid,<sup>64</sup> and polymer<sup>71</sup>) and were demonstrated even to pass through an organic polymer membrane of  $\sim 120$  μm thickness.<sup>68</sup> The desorption of OH radicals is also allowed at the TiO<sub>2</sub>/water interface, which was confirmed by a recent study that observed the diffusing ·OH<sub>f</sub> from the illuminated TiO<sub>2</sub> surface in water through a gap of 7.5 μm using a single molecule detection technique based on total internal reflection fluorescence microscopy (TIRFM).<sup>74</sup> In PCO processes, the hole and ·OH<sub>s</sub> react mainly with adsorbed substrates and the desorption of intermediates from the surface should inhibit further mineralization. On the other hand, mobile ·OH<sub>f</sub> can react with both surface-bound and unbound substrates/intermediates and is a more versatile oxidant. The ·OH<sub>f</sub> diffusing from the irradiated anatase TiO<sub>2</sub> into the aqueous bulk was observed while that was not observed with rutile as shown in Fig. 2a and b. Therefore, the PCO on rutile is largely limited to the adsorbed substrates, whereas the working range of PCO on anatase is more expanded owing to the presence of mobile ·OH (Fig. 2c). This mechanism was newly suggested as an explanation for the common observations that anatase has higher activities than rutile for many PCO reactions. Therefore, as for the photocatalytic reductive conversion that does not involve the hydroxyl radical, the intrinsic activities of anatase and rutile are little different.<sup>73</sup> However, why anatase allows the desorption of ·OH<sub>f</sub> and rutile does not and what properties of the TiO<sub>2</sub> surface control the desorption of the active radical at the molecular level are not understood and need to be further explored.

The generation of OH radicals can be changed by modifying the surface of the semiconductor. The surface adsorption of inorganic anions (fluorides, phosphates, and sulfates) may be the simplest method.<sup>75,76</sup> The surface fluorination of TiO<sub>2</sub>, which replaces the surface hydroxyl group with fluoride (reaction (2)),<sup>77–82</sup> was suggested to prefer the generation of ·OH<sub>f</sub> to ·OH<sub>s</sub> because VB holes react mainly with the adsorbed water molecules (not the surface hydroxyl group) under the condition that the surface hydroxyl groups are depleted by the fluoride substitution:<sup>83</sup>



The surface fluorination also hinders the direct VB hole transfer pathway when the presence of surface fluoride inhibits the adsorption of substrates.<sup>75,77–80</sup> Free OH radicals that desorb from the TiO<sub>2</sub> surface have high mobility and diffusivity in the aqueous solution.<sup>8,51,72</sup> Hence, the photocatalytic decompositions of phenol,<sup>75</sup> TMA,<sup>62</sup> and acid orange 7<sup>75</sup> were enhanced

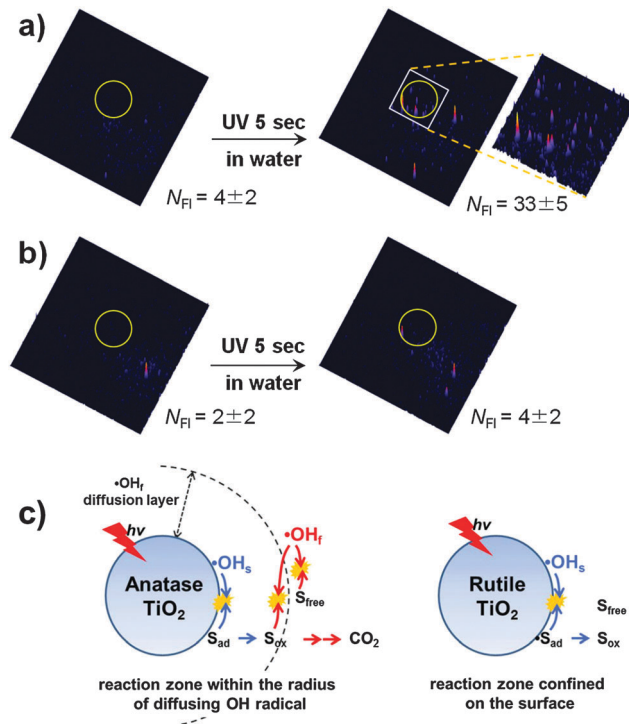


**Fig. 2** (a and b) Fluorescence images of free hydroxyl radicals ( $\cdot\text{OH}$ ) that migrated through a gap from the UV-illuminated  $\text{TiO}_2$  (a: anatase, b: rutile) to HPF-coated cover glass. The  $\text{TiO}_2/\text{water}$  system with silanol-modified HPF (3'-( $\rho$ -hydroxyphenyl)fluorescein) was compared before (left) and after (right) UV irradiation for 5 s. The diffusion gap is 7.5  $\mu\text{m}$ . The UV irradiation region is inside the yellow circle in the images. NFI indicates the number of fluorescence signals. The size of the image is 50 × 50  $\mu\text{m}$ . (c) Illustration of OH-radical-mediated photocatalysis on anatase and rutile. Reprinted with permission from ref. 74 (Copyright 2014 Wiley-VCH Verlag GmbH & Co. KGaA, Weinheim).

on the fluorinated  $\text{TiO}_2$ . On the other hand, the hole transfer-mediated oxidations are significantly retarded because the adsorption or surface complexation of substrates is usually inhibited on the fluorinated surface.<sup>75</sup> Such enhanced OH radical-mediated pathway on the fluorinated surface was further confirmed by the highly accelerated photocatalytic degradation of stearic acid film that is remotely located ~150  $\mu\text{m}$  away from the fluorinated  $\text{TiO}_2$  surface through the air.<sup>65</sup> The adsorption of phosphates and sulfates on  $\text{TiO}_2$  may exhibit similar effects<sup>76,79,80</sup> despite the difference in the working pH region, effectiveness, and stability.

**2.1.3. Conduction band (CB) electrons.** Although the VB holes and OH radicals are the main active species in most PCO processes, their roles are effective only when the CB electrons are also efficiently transferred on the illuminated semiconductor surface. Otherwise, the accumulation of CB electrons results in the fast recombination with VB holes or surface-bound OH radicals, which reduces the overall photocatalytic efficiencies. As for  $\text{TiO}_2$ , the CB edge is located at *ca.* −0.51 V (at pH 7), which gives CB electrons a mild reducing power. In most PCO processes, molecular oxygen dissolved in water or in ambient air serves as a scavenger of CB electrons ( $E^\circ(\text{O}_2/\text{O}_2^\bullet^-) = -0.33 \text{ V}$ ). The presence of alternative electron acceptors such as  $\text{Fe}^{3+}$ ,<sup>37,84,85</sup>

$\text{Ag}^+$ ,<sup>86,87</sup>  $\text{H}_2\text{O}_2$ ,<sup>88,89</sup>  $\text{S}_2\text{O}_8^{2-}$ ,<sup>88,90–92</sup>  $\text{BrO}_3^-$ ,<sup>88,90</sup>  $\text{IO}_4^-$ ,<sup>88,90,91</sup> and polyoxometalate (POM)<sup>37,85,93–96</sup> may accelerate the photocatalytic processes and enable some photocatalytic processes even in the absence of  $\text{O}_2$ . While the transfer of CB electrons to  $\text{O}_2$  induces the generation of ROS such as superoxide and hydrogen peroxide, the direct CB electron transfer to some substrates may induce their reductive transformation or degradation. For example, perhalogenated compounds such as carbon tetrachloride ( $\text{CCl}_4$ ),<sup>97,98</sup> trichloroacetate ( $\text{CCl}_3\text{CO}_2^-$ ; TCA),<sup>99</sup> and perfluoroctanesulfonic acid (PFOS)<sup>100–103</sup> hardly react with the VB holes and OH radicals because of the lack of the oxidizable functional groups such as C–H bonds and unsaturated bonds. Such compounds should be reductively degraded through CB electron transfers (*e.g.*, see reaction (3)). The CB electron transfer part is also critical in the transformation of inorganic substances such as inorganic oxyanions and metal ions. A typical example is the reductive transformation of toxic metal ions to lower oxidation states (*e.g.*,  $\text{Cr}(\text{vi}) \rightarrow \text{Cr}(\text{iii})$ )<sup>104,105</sup> or to the zero-valent metallic state (*e.g.*,  $\text{Ag}(\text{i}) \rightarrow \text{Ag}^0$ )<sup>104,105</sup> through successive single electron transfers.<sup>106,107</sup>

The electron transfer part can also be controlled by modifying the  $\text{TiO}_2$  surface. Surface platinization is the most commonly employed technique for enhancing the CB electron transfer.<sup>108</sup> When Pt is deposited onto  $\text{TiO}_2$  with creating a Schottky barrier at the interface,<sup>109</sup> the Pt phase on  $\text{TiO}_2$  serves as an electron sink, facilitating the charge separation and retarding charge recombination. The enhanced electron transfer on Pt-deposited  $\text{TiO}_2$  has been demonstrated in many cases. The electron shuttles (*e.g.*,  $\text{Fe}^{3+}/\text{Fe}^{2+}$  redox couple) present in the illuminated suspension of semiconductor particles can generate current on a collector electrode and the deposition of Pt on suspended  $\text{TiO}_2$  particles markedly enhanced the photocurrent (Fig. 3), which demonstrates the role of Pt in facilitating the interfacial electron transfer.<sup>37</sup> The accelerated dechlorination of  $\text{CCl}_4$  in dye-sensitized Pt/ $\text{TiO}_2$  suspensions is also a good evidence of the role of Pt as an electron transfer mediator.<sup>97,98</sup>

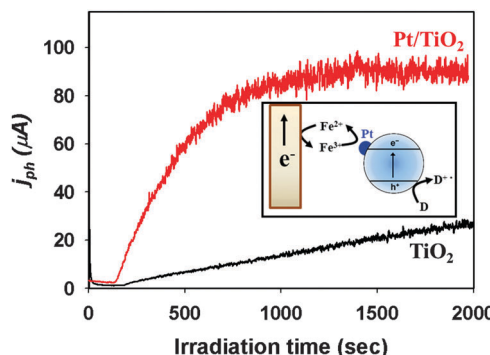


**Fig. 3** Comparison of  $\text{Fe}^{3+}$ -mediated photocurrents collected on a Pt electrode for  $\text{TiO}_2$  and Pt/ $\text{TiO}_2$ . The inset shows the current collection on an inert Pt electrode immersed in a UV-illuminated Pt/ $\text{TiO}_2$  suspension. Adapted with permission from ref. 150 (Copyright 2014 American Chemical Society).



The scavenging of electrons in Pt subsequently accelerates the hole-mediated oxidation part as demonstrated in numerous cases.<sup>8,79,99,110–115</sup> The overall transfer of electrons and holes on semiconductor nanoparticles should be balanced to maintain the charge neutrality. However, the role of Pt is more complex than that of a simple CB electron sink. The presence of Pt not only accelerates the photocatalytic reaction rate but also changes the reaction pathways to generate different products because of the well-known thermal catalytic activity of Pt.<sup>99,114,116</sup> In addition, the effects of Pt on the photocatalysis rate are not always positive and negative effects were also reported.<sup>99,115</sup> To make the matter more complex, the reported effects of Pt on the photocatalytic degradation of a specific substrate are often contradictory.<sup>117–121</sup> In other words, the effects of Pt are highly substrate-specific and depend on the Pt–substrate interaction as well as the intrinsic properties of Pt (size, oxidation state, *etc.*). For example, the oxidation state of Pt critically influences the initial degradation rate of trichloroethylene (TCE).<sup>115</sup> While the photocatalytic activity of  $\text{Pt}^0/\text{TiO}_2$  is almost similar to that of bare  $\text{TiO}_2$ ,  $\text{TiO}_2$  loaded with oxidized Pt ( $\text{Pt}_{\text{ox}}$ ) exhibits negligibly low activity. It was proposed that TCE adsorbed on  $\text{Pt}_{\text{ox}}$  chemically mediates the charge recombination through the redox cycle of TCE. The platinization of  $\text{TiO}_2$  and other semiconductors as a means of enhancing the photocatalytic activity has been very popular, but the overall effects are rather complex and not easy to be generalized. It depends on how the platinumized samples are prepared, what are the experimental conditions, and what are the substrates. The effects of the presence of Pt on the semiconductor photocatalytic reactions, though widely practiced and popular, still need to be understood at the molecular level.

**2.1.4. Superoxide and hydroperoxy radical.** The formation of superoxide ( $\text{O}_2^-$ ) through a CB electron transfer to  $\text{O}_2$  is thermodynamically favorable since the  $\text{TiO}_2$  CB edge potential ( $-0.51$  V at pH 7) is slightly more negative compared to the reduction potential of  $\text{O}_2$  ( $-0.33$  V). With increasing pH, the position of the CB edge moves by  $-59$  mV per unit pH (Nernstian behavior) owing to the amphoteric nature of the surface hydroxyl groups on  $\text{TiO}_2$ , whereas the reduction potential of  $\text{O}_2$  is unchanged. As a result, the thermodynamic driving force for electron transfer becomes greater with increasing pH. With decreasing pH, hydroperoxy radicals ( $\text{HO}_2^\bullet$ ) become the predominant species, owing to the acid–base equilibrium between  $\text{HO}_2$  and  $\text{O}_2^-$  ( $\text{HO}_2 \leftrightarrow \text{O}_2^- + \text{H}^+$ ;  $pK_a = 4.8$ ).<sup>122</sup> From the kinetics point of view, the CB electron transfer to  $\text{O}_2$  is much slower ( $\sim$  milliseconds) than that of hole transfer ( $\sim$  100 nanoseconds) at the  $\text{TiO}_2$  interface, suggesting that the CB electron transfer part can limit the overall PCO reaction rate.<sup>4,123,124</sup>

The superoxide/hydroperoxy radical is generally a much weaker oxidant than the VB hole and OH radical, but it can serve as an important oxidant in some cases. An outstanding example is the PCO of arsenite ( $\text{As}^{III}$ ) to arsenate ( $\text{As}^V$ ).<sup>96,125–129</sup> It has been proposed<sup>96,126,127,129,130</sup> and later verified<sup>125,128</sup> by time-resolved transient absorption spectroscopy that the arsenite adsorbed on  $\text{TiO}_2$  serves as an external charge-recombination center, where the reaction of arsenite with holes

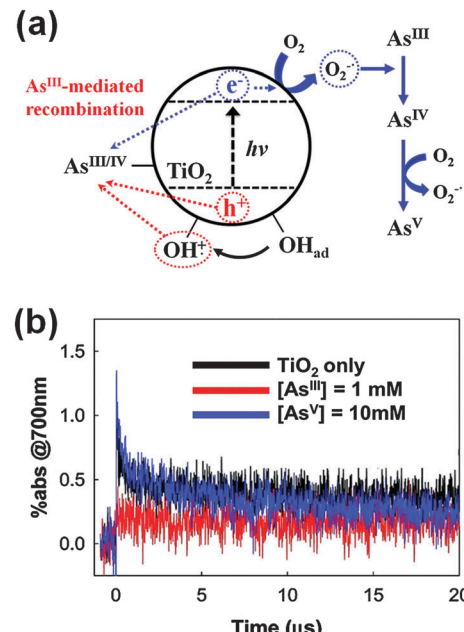


Fig. 4 (a) Schematic illustration of  $\text{As}^{III}$  as an external charge recombination center on UV-excited  $\text{TiO}_2$ . (b) Transient absorption time traces (at 700 nm) of  $\text{TiO}_2$  slurry in the presence of  $\text{As}^{III}$  or  $\text{As}^V$ . Reprinted with permission from ref. 125 (Copyright 2010 American Chemical Society).

and OH radicals is immediately followed by a CB electron transfer (Fig. 4). Although the trapped electron transfer to  $\text{O}_2$  is slow ( $> 20 \mu\text{s}$ ) and the homogeneous bimolecular rate constant between the superoxide and arsenite is as low as  $10^6 \text{ M}^{-1} \text{ s}^{-1}$ , the presence of the  $\text{As}^{IV}/\text{As}^{III}$  redox couple-mediated null cycle makes the superoxide-mediated oxidation path important in the photocatalytic conversion of  $\text{As}^{III}$  to  $\text{As}^V$ . The modification of the  $\text{TiO}_2$  surface may enhance the electron transfer to  $\text{O}_2$  and inhibits the  $\text{As}^{IV}/\text{As}^{III}$  couple-mediated null cycle with significantly changing the PCO kinetics of arsenite. For example, the loading of co-catalysts such as Pt on  $\text{TiO}_2$  facilitates the electron transfer to  $\text{O}_2$  with enhancing the generation of superoxide and accelerating the PCO of arsenite.  $\text{TiO}_2$  hybridized with reduced graphene oxide (rGO) works similarly as  $\text{Pt}/\text{TiO}_2$  and facilitates the transfer of photo-generated electrons from  $\text{TiO}_2$  CB to  $\text{O}_2$ , which subsequently hinders the  $\text{As}^{IV}/\text{As}^{III}$ -mediated recombination and enhances the overall arsenic oxidation.

**2.1.5. Hydrogen peroxide.** The solar photocatalytic production of hydrogen peroxide ( $\text{H}_2\text{O}_2$ ) is interesting in view of both environmental and energy applications. It is not only a widely used oxidant in water treatment processes but also a valuable fuel itself with a high energy content. Hydrogen peroxide is generated by the proton-coupled electron transfer to superoxide and hydroperoxy radical ( $E^\circ(\text{HO}_2^\bullet/\text{H}_2\text{O}_2) = 1.007$  V at pH 7). It can also be produced from the recombination of two OH radicals, but this process is a minor pathway in aqueous photocatalytic systems.<sup>131</sup> In contrast to  $\text{ZnO}$ , the amount of  $\text{H}_2\text{O}_2$  produced on  $\text{TiO}_2$  is very small ( $< 0.1 \mu\text{M}$ ) even in the presence of organic electron donors, because it forms the surface peroxy species on  $\text{TiO}_2$  which is immediately degraded under irradiation.<sup>17,132</sup>



The photocatalytic production of  $\text{H}_2\text{O}_2$  can be significantly enhanced by either facilitating the interfacial electron transfer or suppressing the adsorption of *in situ* generated  $\text{H}_2\text{O}_2$ . For example, Au nanoparticles loaded on  $\text{TiO}_2$  facilitate the reduction of molecular oxygen,<sup>133</sup> while the surface fluorides on  $\text{TiO}_2$  effectively inhibit the formation of surface peroxide species,<sup>82</sup> both of which significantly enhance the overall production of  $\text{H}_2\text{O}_2$  under UV irradiation. The *in situ* produced  $\text{H}_2\text{O}_2$  can be decomposed into hydroxyl radicals and hydroperoxyl radicals *via* further electron transfer, direct photolysis, or a Fenton-like reaction. It should be noted that  $\text{H}_2\text{O}_2$  itself serves as both an electron acceptor and an electron donor on illuminated  $\text{TiO}_2$ . Therefore, the photocatalytic decomposition of  $\text{H}_2\text{O}_2$  is not retarded at all in the absence of  $\text{O}_2$ .<sup>134</sup> As a result of  $\text{H}_2\text{O}_2$  decomposition at the irradiated  $\text{TiO}_2$ /air interface,  $\text{HO}_2$  radicals are produced as an intermediate, some of which desorb from the  $\text{TiO}_2$  surface into the gas phase.

## 2.2. Multiple charge-transfers

**2.2.1. Proton-coupled electron transfers (PCETs).** The photocatalytic production of  $\text{H}_2$  and hydrocarbons through water splitting and  $\text{CO}_2$  reduction requires a series of proton-coupled electron transfers (Fig. 5). For example, two electron transfers are necessary for the production of  $\text{H}_2$  from water, whereas two, four, six, and eight electron transfers are required for the production of formate, formaldehyde, methanol, and methane from  $\text{CO}_2$ , respectively. From a thermodynamic point of view, multi-electron transfer is more favorable than single electron transfer (*e.g.*,  $E^\circ(\text{CO}_2/\text{HCOOH}) = 0.197 \text{ V}$ ) vs.  $E^\circ(\text{CO}_2/\text{CO}_2^{\bullet-}) = -1.9 \text{ V}$ ).<sup>135–139</sup>

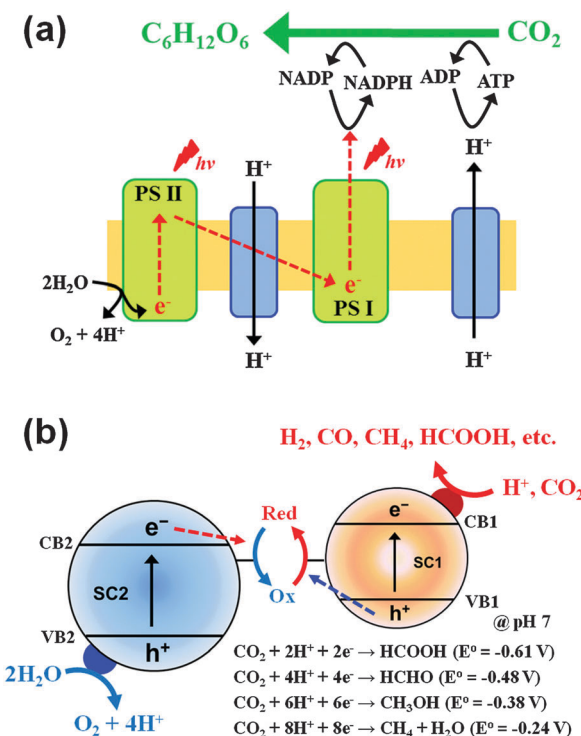


Fig. 5 Schematic illustration of the multiple charge transfers occurring in (a) photosynthesis and (b) artificial photosynthesis (Z-scheme).

However, the former is kinetically and stochastically hindered primarily because the supply of electrons is limited by the flux of incident photons under solar irradiation conditions (not allowing simultaneous multi-photon absorption by a single semiconductor particle) and the lifetime of the charge transfer intermediates is usually not long enough to wait for the next available electron. As a result, the PCETs should proceed through a series of single electron transfer events, which indicates that the overall photoconversion should involve several intermediates through the sequential electron transfers. The intermediates are usually unstable and short-lived and are subject to the attack from VB holes and OH radicals before reacting with the next electron, which nullifies the overall photoconversion process. On the other hand, unlike the case of water reduction in which  $\text{H}_2$  is the sole product, the selectivity control among various  $\text{CO}_2$  reduction products remains a big challenge. The electrochemical reduction potentials of  $\text{CO}_2$  through two to eight electron transfers (resulting in diverse products; see Fig. 5) fall in a narrow potential range of  $\sim 0.4 \text{ V}$  and the preferential control for a specific product is difficult thermodynamically. Therefore, the development of catalytic materials for the product selectivity in PCET processes is highly desired.

**2.2.2. Catalysts for PCETs.** The surface properties of semiconductors have been modified to facilitate and control the multi-electron transfers.  $\text{TiO}_2$  is activated only by UV irradiation and its theoretical solar conversion efficiency for hydrogen production (*i.e.*, solar-to-hydrogen (STH) efficiency) is only  $\sim 1\%$ .<sup>140</sup> The CB electron in  $\text{TiO}_2$  has only mild reduction power, which is not very suitable for the synthesis of solar fuels. However,  $\text{TiO}_2$  is still frequently employed as a base material in the solar fuel production owing to the excellent stability, low cost, and low toxicity of the material. To accelerate the multiple CTs, noble metal nanoparticles (Pt, Au, Ag, Ru, and Rh) are often deposited on semiconductor surfaces, which serve as a reservoir of electrons. Among them, Pt shows the best performance for  $\text{H}_2$  evolution due to its ability to attract and store electrons and its optimal catalytic activity for  $\text{H}_2$  formation and desorption.<sup>45,141,142</sup>

The presence of Pt is often essential for multi-CTs but its high cost hinders its widespread practical applications. Alternative co-catalytic materials consisting of earth-abundant elements are being actively sought and carbon-based materials including carbon nanotubes,<sup>33,35,143,144</sup> graphite,<sup>145</sup> and graphene<sup>146</sup> have been frequently investigated for this purpose. Such carbon-based materials have unique electronic properties, owing to the conjugated  $\text{sp}^2$  carbon networks facilitating CT.<sup>147</sup> For example, reduced graphene oxide (rGO) was shown to serve as an electron reservoir in  $\text{TiO}_2$  photocatalysis, retarding the recombination of charge pairs and leading to enhanced photoconversion efficiency (Fig. 6).<sup>145,148,149</sup> In a typical preparation of the  $\text{TiO}_2$ /rGO hybrid,  $\text{TiO}_2$  particles were loaded on the rGO sheet but different geometrical arrangements between rGO and  $\text{TiO}_2$  particles have a strong influence on the photocatalytic activity.<sup>147,150,151</sup> The hybridization of nanometer-sized GOs and  $\text{TiO}_2$  nanoparticles induces a self-assembled core/shell structure which highly enhances the interfacial contact between them in comparison with the particles-on-a-sheet geometry. GO in direct contact with



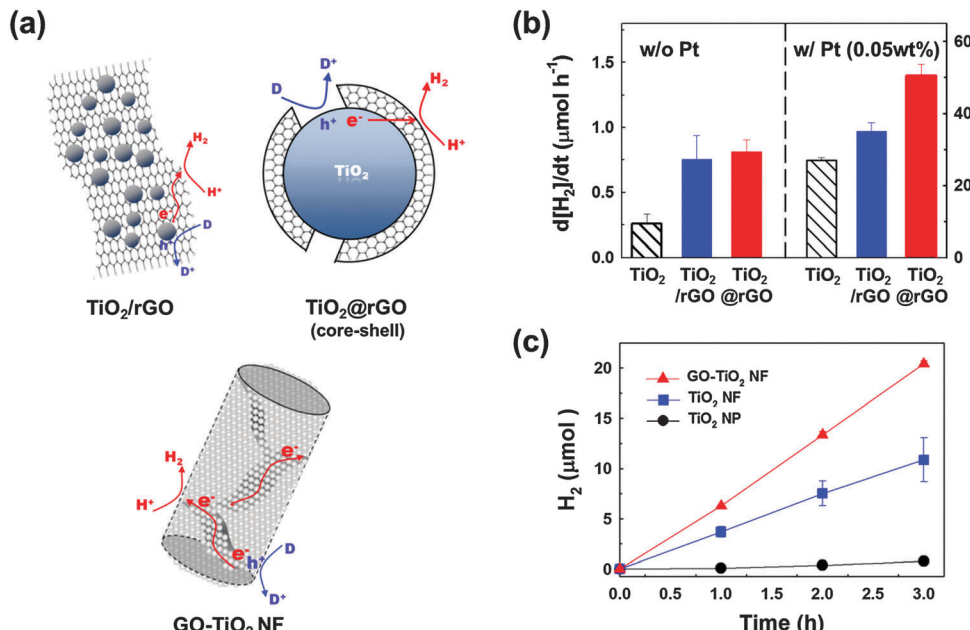


Fig. 6 (a) Illustration of the various composite structures of  $\text{TiO}_2$  and (r)GO sheets and the associated charge transfers for hydrogen production. (b) Photocatalytic  $\text{H}_2$  production rates in the aqueous suspensions of  $\text{TiO}_2$ ,  $\text{TiO}_2$  dispersed on a 2D rGO sheet, and the  $\text{TiO}_2/\text{rGO}$  core/shell structure before (left panel) and after Pt loading (right panel). (c) Time profiles of  $\text{H}_2$  production in the aqueous suspensions of  $\text{TiO}_2$  nanoparticles (NPs),  $\text{TiO}_2$  nanofibers (NFs), and GO embedded in  $\text{TiO}_2$  NFs ( $\text{GO}-\text{TiO}_2$  NF). (a and b) Adapted with permission from ref. 149 (Copyright 2012 American Chemical Society). (a and c) Reprinted from ref. 152 with permission by Elsevier.

$\text{TiO}_2$  can be photocatalytically reduced, which leads to the formation of  $\text{TiO}_2/\text{rGO}$  core/shell (Fig. 6a). This composite clearly differentiates itself from the conventional  $\text{TiO}_2/\text{rGO}$  composite that is based on the larger  $\mu\text{m}$ -sized rGO sheet (particles-on-a-sheet:  $\text{TiO}_2/\text{rGO}$  sheets). The photocatalytic activities of the core/shell are significantly higher than those of bare  $\text{TiO}_2$  for hydrogen production (Fig. 6b). In another geometry,  $\text{TiO}_2$  nanofibers (NFs) in which GO sheets were incorporated within the NF matrix ( $\text{GO}-\text{TiO}_2$  NFs) were also prepared and tested for their photocatalytic and PEC activities (Fig. 6a). The GO sheets embedded in  $\text{TiO}_2$  NFs improve the interparticle connection and facilitate the charge pair separation by serving as an in-built electron conduit with enhancing the photoactivity (Fig. 6c).<sup>152</sup> Even though the photocatalytic activities of  $\text{TiO}_2$  hybridized with various forms of carbon nanomaterials are higher than those of bare  $\text{TiO}_2$  in many reported cases including the above examples, they are usually lower than those of Pt/TiO<sub>2</sub>. However, the co-presence of carbon nanomaterials along with Pt further enhances the photocatalytic activities of Pt/TiO<sub>2</sub>. The simultaneous loading of Pt and rGO on  $\text{TiO}_2$  (ternary hybrid) markedly enhanced the photocatalytic production of  $\text{H}_2$ , as compared to the binary hybrids (Pt/TiO<sub>2</sub> and  $\text{TiO}_2/\text{rGO}$ ) (Fig. 6b). This indicates that rGO can act as an auxiliary co-catalyst, thereby reducing the amount of expensive Pt required for  $\text{H}_2$  production.

In addition, rGO was found to be an excellent catalyst to drive the photocatalytic production of  $\text{H}_2\text{O}_2$  in aqueous  $\text{TiO}_2$  suspension.<sup>151</sup> rGO/TiO<sub>2</sub> displayed the highest photocatalytic activity in producing  $\text{H}_2\text{O}_2$  (*via* PCETs to molecular oxygen) in aqueous 2-propanol solution compared with noble metal-loaded

$\text{TiO}_2$  (Fig. 7a). The leveling-off of  $\text{H}_2\text{O}_2$  production is attributed to the *in situ* decomposition of produced  $\text{H}_2\text{O}_2$  and the relevant kinetics can be expressed with  $[\text{H}_2\text{O}_2] = (k_f/k_d)[1 - \exp(-k_d t)]$  ( $k_f$  and  $k_d$  refer to the formation and decomposition rate constants, respectively).<sup>131,153</sup> According to the kinetic analysis,  $k_f$  with rGO/TiO<sub>2</sub> was not the largest, whereas  $k_d$  with rGO/TiO<sub>2</sub> was the smallest, leading to the highest net yield of  $\text{H}_2\text{O}_2$  production. The photocatalytic decomposition of  $\text{H}_2\text{O}_2$  can be further retarded by adsorbing phosphate on rGO/TiO<sub>2</sub> because the adsorbed phosphate inhibits the adsorption of  $\text{H}_2\text{O}_2$  (Fig. 7b). When  $\text{Co}^{2+}$  was present together with phosphate, cobalt-phosphate complexes (CoPi) were *in situ* formed on rGO/TiO<sub>2</sub> (Fig. 7c). The ternary rGO/TiO<sub>2</sub>/CoPi produced  $\text{H}_2\text{O}_2$  at  $\sim 80 \mu\text{M}$  in the absence of any sacrificial hole scavenger, which was far more efficient than rGO/TiO<sub>2</sub> (Fig. 7b).

Other materials can be employed as a modifier of  $\text{TiO}_2$  for enhancing the multiple CTs. For the conversion of  $\text{CO}_2$  to hydrocarbons, for example, a thin Nafion layer can be coated on the Pd/TiO<sub>2</sub> nanoparticles to facilitate PCETs as well as to inhibit the re-oxidation of the intermediates and products.<sup>154</sup> It was found that the introduction of the Nafion layer enhanced the production of methane, ethane, and propane in UV-irradiated Pd/TiO<sub>2</sub> suspensions. The effect of the Nafion overlayer on  $\text{TiO}_2$  seems to be related to its roles to maintain the local proton activity within the layer to facilitate PCET reactions (as a proton conductor) and to inhibit the photooxidation of the intermediate products of  $\text{CO}_2$  reduction (as a barrier layer for the oxidation of reaction intermediates). The Nafion layer may stabilize the intermediates, inhibit the re-oxidation of the  $\text{CO}_2$  reduction products, and subsequently may assist in the

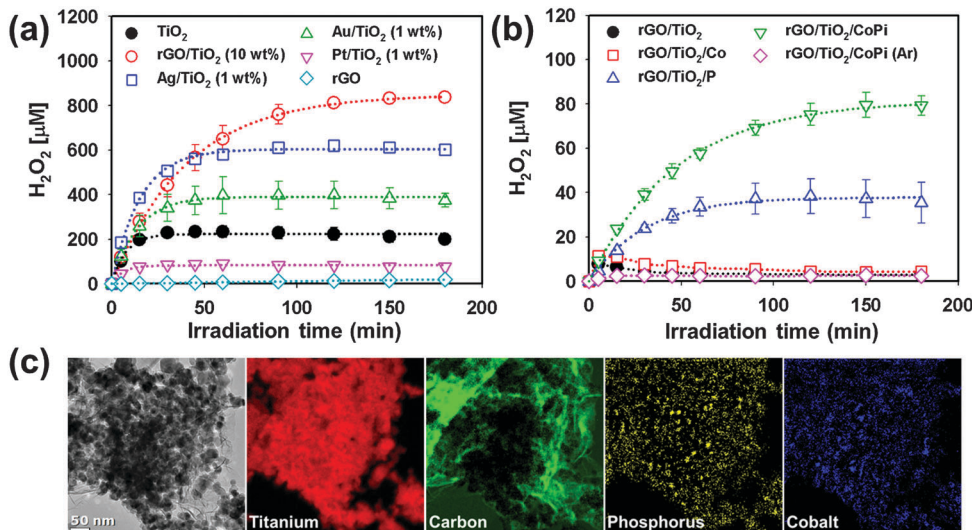


Fig. 7 Photocatalytic production of H<sub>2</sub>O<sub>2</sub> (a) in the presence of 2-propanol and (b) in the absence of 2-propanol as a result of water oxidation. (c) TEM image and EELS mapping of rGO/TiO<sub>2</sub>/CoPi. Reproduced from ref. 151 with permission from The Royal Society of Chemistry.

serial electron transfers to produce the final products. The perfluorinated backbone of Nafion itself resists the photo-oxidation, and therefore, the photoactivity of the Nafion/Pd/TiO<sub>2</sub> composite can be sustained under UV irradiation. Incidentally, owing to the cation exchange property of Nafion, the Nafion-coated TiO<sub>2</sub> has also been employed as a photocatalyst that selectively adsorbs cationic substrates or cationic sensitizers.<sup>94,95</sup>

To achieve the overall photoconversion, the PCET half reactions should be coupled with the oxidation half reactions which supply the protons and electrons. The most ideal counterpart should be the oxidation of water, which also involves the multi-electron transfers (requiring four proton/electron couples) and should also be limited by the photon flux. The photooxidation of water is an important building block in photosynthesis because it is the only reaction that can supply the electrons and protons for a global-scale production of solar fuels.<sup>17,155–157</sup> Although the VB holes in most oxide semiconductors have the oxidation potential high enough to drive water oxidation, the water oxidation part always kinetically limits the overall photoconversion. In most photocatalytic oxidation processes occurring on bare metal oxide semiconductors, the oxidation of water preferentially generates the transient hydroxyl radical species which has little chance to be further oxidized to O<sub>2</sub> *via* multiple hole transfers. To overcome this problem, water oxidation catalysts such as cobalt phosphate (CoPi) and nickel borate (NiBi) complexes can be deposited on the semiconductor electrode (mostly non-TiO<sub>2</sub> electrodes such as BiVO<sub>4</sub>).<sup>29,30,158</sup> The application of anodic biases to the semiconductor electrode oxidizes the deposited cobalt(II) and nickel(II) species (*e.g.*, Co<sup>2+</sup> + 2H<sup>+</sup> → Co<sup>4+</sup>), which form complexes with phosphate and borate under illumination. The oxidized species then return to their original oxidation state through oxidizing water (*e.g.*, Co<sup>4+</sup> + H<sub>2</sub>O → Co<sup>2+</sup> + 1/2O<sub>2</sub> + 2H<sup>+</sup>). Although this catalytic material is composed of earth-abundant elements and easy to be prepared, it can serve as a charge recombination center because of the sluggish

interfacial hole transfer under certain conditions (*e.g.*, large anodic bias, thick coat, *etc.*).<sup>29,41</sup> Incidentally, the water photo-oxidation on semiconductor electrodes can also be enhanced by passivation of the semiconductor surface by a thin insulating overlayer, which reduces the number of electron trapping sites on the semiconductor surface, thereby facilitating water photooxidation despite the insulating nature of the overlayer (*e.g.*, a thin Al<sub>2</sub>O<sub>3</sub> overlayer on the WO<sub>3</sub> photoanode surface).<sup>159</sup>

### 3. Interparticle charge transfers

Efficient charge separation can be achieved by interparticle CTs through particle-to-particle junctions. The interparticle CT reduces the chance of charge recombination and eventually increases the overall photocatalytic activities. It occurs both in single semiconductor systems (*e.g.*, agglomerates of colloidal nanoparticles<sup>160,161</sup> and compactly packed nanoparticles<sup>162,163</sup>) and in hybrid semiconductor-composite systems (binary<sup>26,32,164,165</sup> and ternary hybrids<sup>25</sup>). Colloidal or suspended semiconductor particles exist almost always as agglomerates in aqueous solution. Hence, the effects of the agglomerate state on the charge separation and transfer need to be carefully considered. The agglomeration of semiconductor particles is usually thought to have a negative effect on the photocatalytic activity because of the reduced surface area and the enhanced light scattering loss. However, the overall effect of agglomeration seems to be more complex than thought.

#### 3.1. Homojunction semiconductor systems

A recent study reported that the photocatalytic H<sub>2</sub> production in TiO<sub>2</sub> suspension containing nitric acid is greatly accelerated after some induction period (Fig. 8a).<sup>160</sup> This unique phenomenon was attributed to the pH increase resulting from the *in situ* photocatalytic reduction of nitrate to ammonia. As the solution

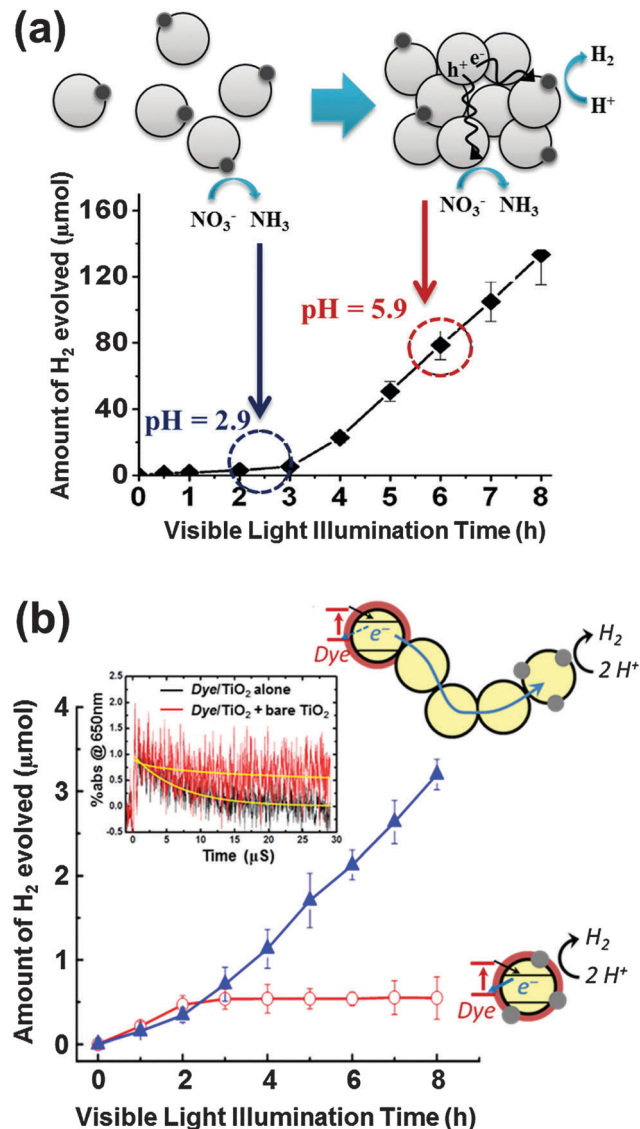


Fig. 8 (a) Time trend of  $\text{H}_2$  evolution in colloidal  $\text{TiO}_2$  synthesized using  $\text{HNO}_3$  and schematic illustration showing well-dispersed colloidal  $\text{TiO}_2$  nanoparticles at pH 2.9 and agglomerated  $\text{TiO}_2$  nanoparticles (pH 5.9). Adapted with permission from ref. 160 (Copyright 2008 American Chemical Society). (b) Schematic illustration and visible light induced production of  $\text{H}_2$  in the aqueous suspension of dye/ $\text{TiO}_2$ /Pt and [dye/ $\text{TiO}_2$  +  $\text{TiO}_2$  +  $\text{TiO}_2$ /Pt]. The inset shows the normalized time traces of absorption at 650 nm (dye $\cdot^+$ ) during the 532 nm laser photolysis of dye/ $\text{TiO}_2$  without bare  $\text{TiO}_2$  and [dye/ $\text{TiO}_2$  + bare  $\text{TiO}_2$ ]. Adapted with permission from ref. 161 (Copyright 2013 American Chemical Society).

pH approaches the zero point charge of  $\text{TiO}_2$  ( $\text{pH}_{zpc} \sim 6.9$ ), a rapid agglomeration of the  $\text{TiO}_2$  colloid is induced, which initiates the production of  $\text{H}_2$ . The colloid agglomeration and the appearance of  $\text{H}_2$  production are coincident. A similar behavior was observed in the case of photocurrent generation (mediated by the  $\text{MV}^{2+}/\text{MV}^+$  redox couple;  $E^\circ = -0.445$  V) in  $\text{TiO}_2$  colloids: a rapid increase in the photocurrent was observed after the agglomeration of  $\text{TiO}_2$  nanoparticles. A plausible explanation is that the charge separation is facilitated by electron hopping from particle to particle when  $\text{TiO}_2$  nanoparticles are connected with

each other within the agglomerates. Hence, the agglomeration-induced acceleration of  $\text{H}_2$  and photocurrent generation are ascribed to the facilitated charge separation by interparticle CT within the agglomerates.

The effect of interparticle CTs in the agglomerates of dye-sensitized  $\text{TiO}_2$  nanoparticles was also systematically studied by using both static photocatalysis and transient laser spectroscopy.<sup>161</sup> A typical dye-sensitized system for  $\text{H}_2$  production includes dye-sensitized  $\text{TiO}_2$  nanoparticles (dye/ $\text{TiO}_2$ ) as a light absorber and platinized  $\text{TiO}_2$  (Pt/ $\text{TiO}_2$ ) as an active catalytic center. Fig. 8b compares two experimental cases of dye sensitization: a common case where the light absorbing dye and the Pt catalyst are on the same nanoparticle (dye/ $\text{TiO}_2$ /Pt) and the other case where each part is separated in different nanoparticles and bare  $\text{TiO}_2$  nanoparticles are added to mediate between two active parts (dye/ $\text{TiO}_2$  +  $\text{TiO}_2$  + Pt/ $\text{TiO}_2$ ). When the light absorbing part of dye/ $\text{TiO}_2$  is separated from the active catalytic center of Pt/ $\text{TiO}_2$ , the role of bare  $\text{TiO}_2$  nanoparticles working as a mediator that connects the above two parts in the agglomerates should be essential. The presence of mediator in the agglomerate indeed facilitated the charge separation (*i.e.*, retarding charge recombination between the oxidized dye and the injected electrons) and the electron transfer from dye/ $\text{TiO}_2$  to Pt/ $\text{TiO}_2$  through multiple grain boundaries subsequently produced more  $\text{H}_2$  (Fig. 8b). A similar phenomenon was also observed in the case of dye-sensitized reduction of Cr(vi) to Cr(III):<sup>161</sup> a notable enhancement of Cr(vi) reduction was observed when bare  $\text{TiO}_2$  nanoparticles were incorporated as a mediator in the dye-sensitized  $\text{TiO}_2$  system. The transient absorption spectroscopic measurements revealed the role of the mediator  $\text{TiO}_2$  nanoparticles by monitoring the transient absorption decay of the photogenerated dye cation (dye $\cdot^+$ ). An increase in the bare  $\text{TiO}_2$  amount (as a mediator in the dye-sensitized  $\text{TiO}_2$  system) enhanced the average lifetimes ( $\tau$ ) of the dye cation by  $\sim 18$  times (from 6.7  $\mu\text{s}$  to 120  $\mu\text{s}$ ) in the aggregated state (Fig. 8b inset).

To utilize the interparticle CT phenomenon in practical applications, particulate mesoporous  $\text{TiO}_2$  (meso- $\text{TiO}_2$ ) with well-ordered pore structures and unique morphologies was developed without the use of templates *via* the hydrothermal method (Fig. 9a).<sup>162</sup> The formation of meso- $\text{TiO}_2$  is governed by the electrostatic potential, which can be controlled by the ionic strength of the solution. By changing the solution ionic strength (*e.g.*, by adding KCl), which controls the hydrolysis of the titanium alkoxide precursor, a mesoporous structure consisting of densely packed nanoparticles was synthesized. The as-synthesized meso- $\text{TiO}_2$  microspheres ( $0.5\text{--}1\ \mu\text{m}$ ) consisting of small primary nanoparticles ( $10\text{--}15\ \text{nm}$ ) exhibit markedly enhanced photo(electro)chemical activities for both  $\text{H}_2$  production and photocurrent generation (through the methyl viologen redox couple in the suspension), compared to colloidal  $\text{TiO}_2$  and commercial  $\text{TiO}_2$  nanoparticles (P25 and Hombikat UV-100). The higher photocatalytic activity of meso- $\text{TiO}_2$  is attributed to the compact packing of  $\text{TiO}_2$  nanoparticles forming uniform agglomerates, which enable the efficient charge separation through the interparticle CT.

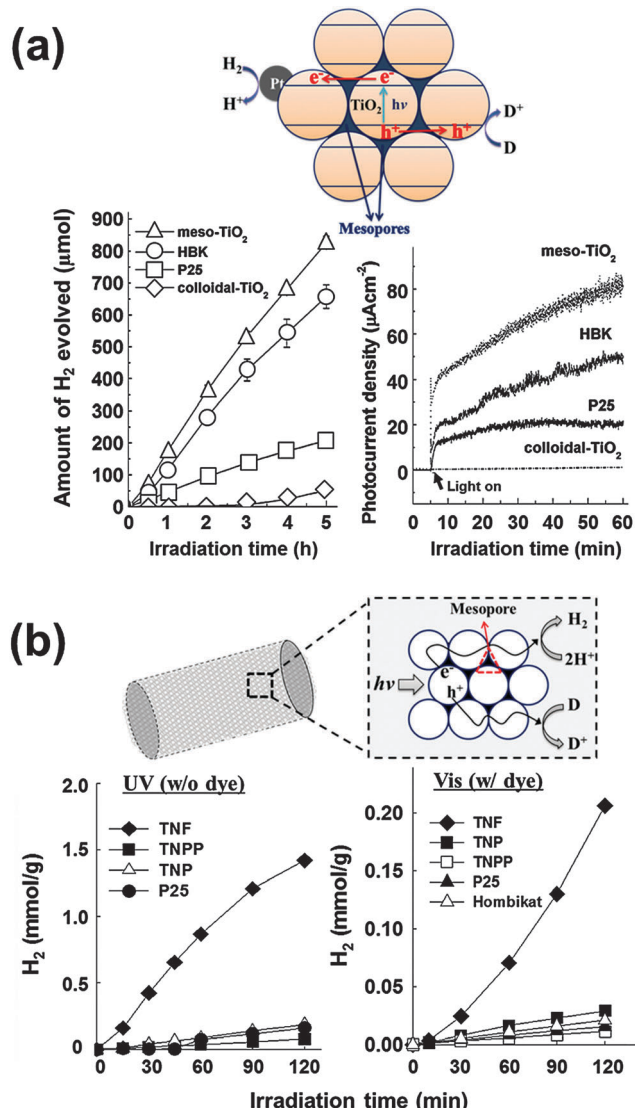


**Fig. 9** (a) Time courses of  $H_2$  evolution and photocurrent generations by different  $TiO_2$  photocatalysts and schematic illustration of mesoporous  $TiO_2$  microspheres. Adapted with permission from ref. 162 (Copyright 2007 American Chemical Society). (b) Time courses of  $H_2$  evolution in aqueous suspensions of  $TiO_2$  nanofibers ( $\lambda > 320$  nm) and dye-sensitized  $TiO_2$  nanofibers ( $\lambda > 420$  nm) with schematic illustration of mesoporous  $TiO_2$  nanofibers. Reproduced from ref. 166 with permission from The Royal Society of Chemistry.

$TiO_2$  fibers consisting of nanoparticles represent another good example of effective interparticle CT. It is well known that electrospinning of pre-crystallized  $TiO_2$  nanoparticles creates well-ordered and aligned high surface area mesoporous  $TiO_2$  nanofibers that are ~500 nm in diameter and a few micrometers in length (Fig. 9b).<sup>163</sup> The photocatalytic activity comparison between the titania nanofibers (TNF) and the nanoparticles (TNP) indicated that the former had 3 times higher activities in photocurrent generation and 7 times higher in  $H_2$  production. The photocatalytic superiority of TNF is attributed to the effects of mesoporosity and nanoparticle alignment, which help efficient charge separation through interparticle CT along the

nanofiber framework. The TNF also exhibited 7 times and >140 times higher dye-sensitized  $H_2$  production, compared to the TNP and commercial  $TiO_2$  samples, respectively.<sup>166</sup> These studies, therefore, provide strong evidence that the charge separation efficiency could be markedly enhanced through interparticle CTs when the individual nanoparticles are directionally arranged with close contacts among them.

### 3.2. Multi-hybrid semiconductor systems with heterojunctions

Combining two different types of semiconductor particles with heterojunctions has been frequently employed as a means of enhancing charge pair separation and thereby enhancing the overall photocatalytic activity.<sup>25,167</sup> A proper selection of semiconductors based on their CB and VB positions leads to the cascaded transfer of photogenerated charge carriers from one semiconductor to another. A variety of binary composites consisting of  $TiO_2$  and other semiconductors (e.g.,  $WO_3$ ,<sup>26,84,168–170  $SnO_2$ ,<sup>171–173</sup>  $ZrO_2$ ,<sup>173</sup>  $CdSe$ ,<sup>174,175</sup> and  $Cds$ <sup>25,32,176,177</sup>) have been prepared and tested for their photocatalytic activities.</sup>

Among the binary  $TiO_2$  composites with heterojunctions,  $WO_3/TiO_2$  composite photocatalysts have been most frequently studied for environmental remediation and solar energy storage.<sup>26,168–170,178–181</sup> The primary role of  $WO_3$  is to accept  $TiO_2$  CB electron. Since  $WO_3$  has a lower (more positive) CB potential than that of the  $TiO_2$  CB, the  $TiO_2$  CB electrons are transferred to the  $WO_3$  CB with reducing  $W(vi)$  to  $W(v)$ . The reduced state of  $WO_3$  (e.g., as a form of  $H_xWO_3$ ) is maintained for a period of time and the stored electrons are slowly released to the surrounding electron acceptors (e.g.,  $O_2$ ) (Fig. 10a).<sup>26,182,183</sup> This photocharge-discharge mechanism has been applied to the corrosion prevention of metals by coating the metal surface with the composite semiconductors. This mechanism was also successfully applied to the conversion of water pollutants (phenol,  $Cr(vi)$ , etc.).<sup>26,168</sup> The coupling of  $TiO_2$  with  $WO_3$  decreased the photocatalytic activities in some cases (e.g., for the gas-phase oxidation of acetaldehyde and the liquid-phase oxidation of 2-naphthol),<sup>178</sup> In addition, the PCO activity of  $WO_3/TiO_2$  for 1,4-dichlorobenzene was shown to be highest only at a certain ratio of  $WO_3$  to  $TiO_2$ , and higher loadings of  $WO_3$  above this fraction decreased the activity significantly.<sup>181</sup> The reduced activity is ascribed to a retarded rate of electron transfer from the  $WO_3$  CB (0.3–0.5 V<sub>NHE</sub>) to  $O_2$ , since its potential is more positive than the  $O_2$  reduction potential ( $E^\circ(O_2/O_2^-) = -0.33$  V<sub>NHE</sub>). This problem can be overcome by loading Pt nanoparticles on  $WO_3$ , which enables the multi-electron reduction of  $O_2$ , which has a more positive potential (e.g.,  $E^\circ(O_2/H_2O_2) = +0.695$  V<sub>NHE</sub> for two-electron reduction) than the one-electron reduction.<sup>184</sup> Consequently, the PCO reactions occurring on  $Pt/WO_3$  were markedly enhanced because the reductive decomposition of  $H_2O_2$  (*in situ* generated from the reduction of  $O_2$ ) produced OH radicals under visible light.<sup>23</sup>

On the other hand, the mismatch of the CB and VB levels in coupling semiconductor systems may reduce their photocatalytic and PEC activities on the contrary. The hybridization of hematite ( $\alpha-Fe_2O_3$ ) on  $TiO_2$  nanotube arrays unexpectedly



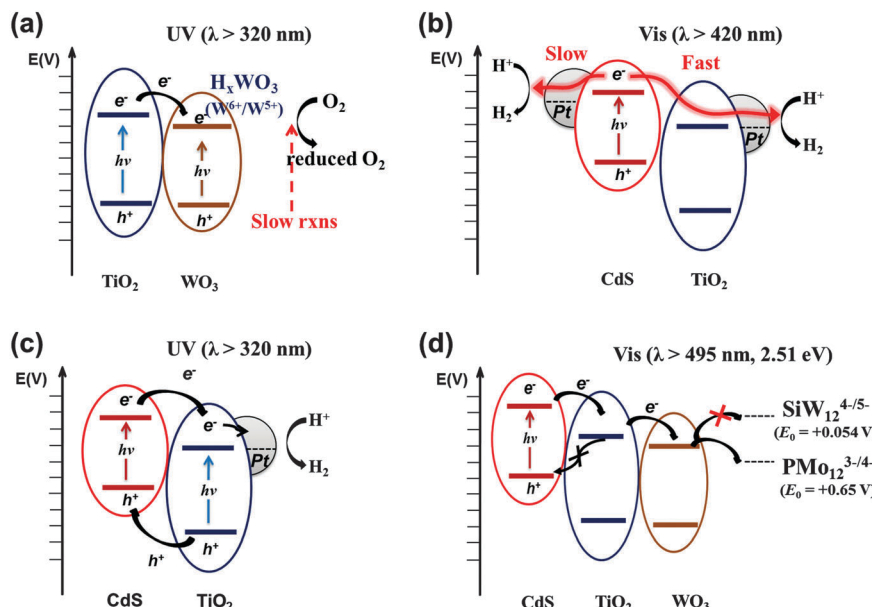


Fig. 10 Schematic illustration of the electron-transfer processes in multi-junction systems under UV and visible light. (a)  $\text{TiO}_2/\text{WO}_3$ , (b and c)  $\text{CdS}/\text{TiO}_2/\text{Pt}$ , and (d)  $\text{CdS}/\text{TiO}_2/\text{WO}_3$ .

decreased PEC and photocatalytic activity (for phenol degradation), primarily due to the low conductivity of hematite and the band position mismatch between  $\text{TiO}_2$  and hematite (the CB and VB of hematite being more positive and negative, respectively, with respect to those of  $\text{TiO}_2$ ).<sup>164</sup> Such mismatch results in enhanced charge recombination.

As for the  $\text{TiO}_2$  hybrid with non-oxide semiconductors,  $\text{CdS}/\text{TiO}_2$  is the most representative example and has been widely applied to the photocatalytic conversion of various substrates such as methane,<sup>185</sup> methyl orange,<sup>186</sup> indole,<sup>187</sup> acid orange II,<sup>188</sup> 1,2,3,4-tetrachlorobenzene,<sup>189</sup> and methylene blue and eosin.<sup>190</sup> The VB and CB of  $\text{CdS}$  are ideally placed in comparison to those of  $\text{TiO}_2$  for efficient charge pair separation and the bandgap of  $\text{CdS}$  is narrow ( $\sim 2.5 \text{ eV}$ ) enough to absorb a substantial portion of solar visible light ( $\lambda \leq 500 \text{ nm}$ ). Upon excitation by visible light, the  $\text{CdS}$  CB electrons are transferred to the  $\text{TiO}_2$  CB, while the holes remain in the  $\text{CdS}$  VB (Fig. 10b). Under optimal conditions, the semiconductor coupling reduces the average emission lifetime of  $\text{CdS}$  by a factor of four (24.6 to 6.8 ns), owing to the scavenging of the CB electrons by  $\text{TiO}_2$ .<sup>191</sup> The electron transfer from  $\text{CdS}$  to  $\text{TiO}_2$  is sensitively influenced by the CB edge potential difference. As the  $\text{CdS}$  particle size decreases to the quantum confinement domain, the bandgap of  $\text{CdS}$  is widened. As a result, the CB edge of  $\text{CdS}$  rises with respect to that of  $\text{TiO}_2$ , which increases the driving force of CB electron transfer from  $\text{CdS}$  to  $\text{TiO}_2$ .<sup>192,193</sup>

The  $\text{CdS}/\text{TiO}_2$  composite can be further modified by noble metal (Pt) nanoparticles. In this ternary configuration (*i.e.*,  $\text{CdS}$ ,  $\text{TiO}_2$ , and noble metal), both semiconductors can be simultaneously excited at different wavelength regions ( $\lambda_{\text{TiO}_2} < 400 \text{ nm}$ ;  $\lambda_{\text{CdS}} > 400 \text{ nm}$ ) due to their different bandgaps. Upon excitation of both  $\text{CdS}$  and  $\text{TiO}_2$ , CB electrons and VB holes are separated to  $\text{TiO}_2$  and  $\text{CdS}$ , respectively, while electrons are effectively

collected at metal nanoparticles (Pt) deposited on  $\text{TiO}_2$  (Fig. 10c). This CT process mimics that of natural photosynthesis<sup>194</sup> in terms of two-photon excitation (PS-II and PS-I in Z-scheme: see Fig. 5a). It is important that Pt is loaded selectively on the  $\text{TiO}_2$  surface only among the  $\text{CdS}/\text{TiO}_2$  composites since the electrons are transferred to the  $\text{TiO}_2$  side. For example, the photoplatinized hybrid of  $\text{CdS}/\text{TiO}_2$  [resulting in  $\text{Pt}-(\text{CdS}/\text{TiO}_2)$  where Pt is loaded on both  $\text{CdS}$  and  $\text{TiO}_2$ ] is much less efficient than the hybrid of  $\text{CdS}/(\text{Pt}-\text{TiO}_2)$  [Pt is photodeposited on  $\text{TiO}_2$  first followed by the deposition of  $\text{CdS}$ ]. The  $\text{CdS}/(\text{Pt}-\text{TiO}_2)$  exhibits 3–30 fold higher  $\text{H}_2$  production compared to  $\text{Pt}-(\text{CdS}/\text{TiO}_2)$ .<sup>32</sup>

Another ideal candidate for a non-oxide semiconductor coupled with  $\text{TiO}_2$  is TaON. The narrow bandgap of TaON ( $\sim 2.4 \text{ eV}$ ),<sup>195</sup> along with the negatively shifted CB and VB edges compared to those of  $\text{TiO}_2$ , induces efficient charge separation at the  $\text{TiO}_2/\text{TaON}$  interface. Nevertheless, there have not been many studies on the coupling of TaON and  $\text{TiO}_2$ , owing to the harsh synthesis conditions of TaON. The synthesis of TaON generally requires high temperature nitridation (at over  $850^\circ\text{C}$ ),<sup>196</sup> which induces particle coarsening and phase transformation of the counter semiconductor (*e.g.*, the transformation of  $\text{TiO}_2$  to  $\text{TiN}$ ).<sup>21,197,198</sup> Recently, a  $\text{TaO}_x\text{N}_y$  thin layer coupled with  $\text{TiO}_2$  nanotubes (TNTs) was prepared by a low temperature nitridation process ( $500^\circ\text{C}$ ) and the TNT composite exhibited much improved PEC water-splitting efficiencies under both visible (3.6 times) and UV (1.8 times) illumination compared to bare TNTs because of the efficient charge pair separation at the heterojunction interface of  $\text{TaO}_x\text{N}_y/\text{TNTs}$  (Fig. 11).<sup>199</sup> In addition, the thin  $\text{TaO}_x\text{N}_y$  layer on TNTs serves as a passivation layer that reduces the surface trap sites and enhances the visible light absorption range.

Ternary hybrid systems have received less attention because of the complexity while the binary systems have been



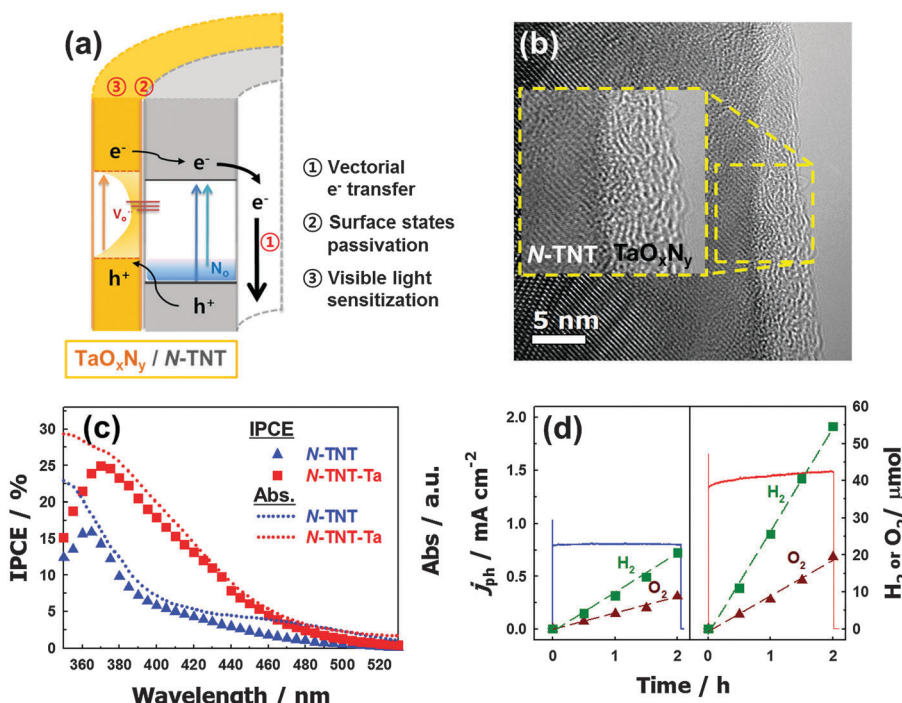


**Fig. 11** (a) Schematic illustration of charge transfers in an *N*-TNT-Ta hybrid. (b) Energy-filtered TEM (EF-TEM) image of an *N*-TNT-Ta hybrid. (c) IPCE spectra of *N*-TNT (triangle) and *N*-TNT-Ta (square) as a function of the incident light wavelength. Dotted lines represent the absorption spectra. (d) Photocurrent transients and the concurrent generation of H<sub>2</sub> and O<sub>2</sub> with *N*-TNT (left panel) and *N*-TNT-Ta (right panel) electrodes polarized at +0.9 V vs. Ag/AgCl under UV illumination ( $\lambda > 320$  nm). Reproduced from ref. 199 with permission from The Royal Society of Chemistry.

extensively studied. To evaluate the effects of the ternary systems, a systematic study was conducted with CdS/TiO<sub>2</sub>/WO<sub>3</sub> hybrids, which have cascaded positioning of the CB edges (see Fig. 10d). In this study, only CdS was selectively excited under the irradiation of  $\lambda > 495$  nm (equivalent to 2.51 eV), in order to focus on the cascaded electron transfer starting from CdS in the ternary hybrid. The photocatalytic reduction of polyoxometalate (POM) ( $E^\circ(\text{PMo}_{12}\text{O}_{40}^{3-/-4-}) = +0.65 \text{ V}_{\text{NHE}}$ ) and PEC tests indicated that the CdS/TiO<sub>2</sub>/WO<sub>3</sub> ternary hybrid has much higher activities compared to bare CdS and binary hybrids (CdS/TiO<sub>2</sub> or CdS/WO<sub>3</sub>) because of the cascaded electron transfer through two sequential heterojunctions (CdS  $\rightarrow$  TiO<sub>2</sub>  $\rightarrow$  WO<sub>3</sub>). Unlike the binary system where the separated charge pairs may recombine directly at the heterojunction, the two sequential heterojunctions along the potential gradient reduce the chance of direct recombination of charge carriers because the electron can be further transferred to the third compartment. The presence of TiO<sub>2</sub> in between CdS and WO<sub>3</sub> provides an energy barrier for the back electron transfer (Fig. 10d). However, the cascaded electron transfer from CdS to TiO<sub>2</sub> to WO<sub>3</sub> reduces the reduction potential of CB electrons progressively, which limits the range of reductive conversions that can be driven by the ternary hybrid photocatalytic system. For example, when tungstosilicate (SiW<sub>12</sub>O<sub>40</sub><sup>4-</sup>), which has a more negative one-electron reduction potential ( $E^\circ = +0.054 \text{ V}_{\text{NHE}}$ ) compared to the WO<sub>3</sub> CB, was used as an alternative POM, the efficiency of the photocatalytic reduction was markedly diminished. The cost of enhancing the charge separation efficiency in the hybrid structure is to make the electrons less energetic.

## 4. Visible light-induced charge transfers

Visible light sensitization of wide bandgap semiconductors like TiO<sub>2</sub> has been intensively investigated as one of the most important research topics in photocatalysis. Unlike the heterojunction semiconductors and impurity-doped semiconductors which are modified primarily by inorganic components, the visible light sensitization of semiconductors can also be achieved by coupling with organic substances. There are two main methods for achieving visible light-induced CT: dye-sensitization<sup>166,200,201</sup> and ligand-to-metal charge transfer (LMCT).<sup>202-211</sup>

### 4.1. Dye sensitization

Dye-sensitization of semiconductor photocatalysts is conceptually similar to the operation mechanism of dye-sensitized solar cells.<sup>15,212</sup> In principle, the dye molecules located at the TiO<sub>2</sub>/solution interface are photoexcited and subsequently inject electrons into the TiO<sub>2</sub> CB (Fig. 12a). These electrons are subsequently transferred to electron acceptors to induce various redox reactions at the semiconductor interface. For effective electron injection from the excited dye to TiO<sub>2</sub>, it is necessary to firmly anchor the dye molecules onto the TiO<sub>2</sub> surface. In aqueous environments, the adsorption of dyes usually proceeds *via* electrostatic interaction with the amphoteric TiO<sub>2</sub> surface ( $>\text{Ti-OH}_2^+ \leftrightarrow >\text{Ti-OH} \leftrightarrow >\text{Ti-O}^-$ ),<sup>4,8</sup> the surface charge of which depends on the solution pH. For example, the most commonly used ruthenium bipyridyl complexes (Ru-bpy) with

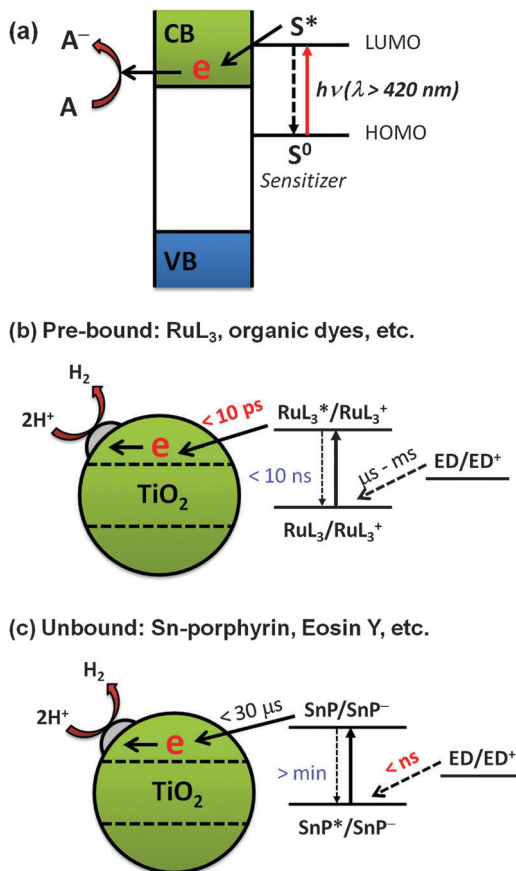


Fig. 12 Schematic illustration of (a) the dye-sensitization mechanism, (b) sensitization by pre-bound dyes, and (c) sensitization by unbound dyes. Reproduced from ref. 217 with permission from The Royal Society of Chemistry.

carboxylate anchoring groups are readily anchored to the TiO<sub>2</sub> surface in the acidic pH region,<sup>97,98,213–215</sup> because the point of zero charge of TiO<sub>2</sub> is at around pH<sub>zpc</sub> ~ 6 (Fig. 12b).<sup>4,8,75</sup> At pH < 6, the surface of TiO<sub>2</sub> is positively charged and attracts the carboxylate anion anchoring groups and the dye anchoring is efficiently achieved. The sensitization of anchored dyes can successfully induce H<sub>2</sub> evolution<sup>201,214,215</sup> and the conversion of water pollutants (e.g., dechlorination of CCl<sub>4</sub> and reduction of Cr<sup>6+</sup>) under visible light.<sup>97,200,201</sup> However, at pH > 6 where the TiO<sub>2</sub> surface is negatively charged, the anionic dyes are electrostatically repelled and the sensitization efficiency decreases.<sup>200,201,213,214</sup> Organic dyes with carboxylate groups also show similar behaviors.<sup>200,201</sup> To widen the working pH range, the carboxylate anchoring group can be replaced with a phosphonate group.<sup>213,216</sup> TiO<sub>2</sub> sensitized with Ru-bpy containing phosphonate groups shows activity for H<sub>2</sub> evolution even at alkaline pH (~9). The number of anchoring groups (carboxylates vs. phosphonates) also significantly influences the photoefficiency and stability of dye-sensitized TiO<sub>2</sub> systems.<sup>213,216</sup> Irrespective of the kind and number of anchoring groups, the pre-adsorption of dyes on TiO<sub>2</sub> is usually required for the initiation of the sensitization.

Interestingly, some studies have shown that the presence of pre-adsorbed dye is not always necessary for dye sensitization

in aqueous environments. One example is the tin(IV)-porphyrin (SnP)-sensitized TiO<sub>2</sub> system (Fig. 12c).<sup>217</sup> SnP has a strong oxidative power due to the high charge on Sn(IV)<sup>218,219</sup> and hence the excited SnP shows a high photoactivity for the oxidation of aqueous organic compounds. Although the adsorption of SnP on TiO<sub>2</sub> is negligible in the pH range of 3–11, a significant amount of H<sub>2</sub> was produced in the SnP/TiO<sub>2</sub> system (turnover number of 410 and quantum efficiency of ~35% at an irradiation wavelength of 550 nm).<sup>217</sup> Laser flash photolysis showed that the free excited SnP is first reduced by an electron donor (e.g., EDTA) owing to its strong oxidation power in the nanosecond time scale. The high charge on Sn(IV) makes the SnP ring highly electrophilic, favoring the formation of the SnP π-radical anion (SnP<sup>•-</sup>). The lifetime of the π-radical anion is long enough (in the order of microseconds) to survive during the slow diffusion from the solution bulk to the TiO<sub>2</sub> surface. As a result, the adsorption of SnP on TiO<sub>2</sub> is not a required condition for H<sub>2</sub> production. This is in contrast with the case of the Ru-bpy/TiO<sub>2</sub> system, where the electron transfer from the electron donor to Ru-bpy is 6–9 orders of magnitude slower than the electron injection from the excited Ru-bpy to TiO<sub>2</sub>.

#### 4.2. Ligand-to-metal charge transfer (LMCT) sensitization

An alternative modification method for visible light activation of TiO<sub>2</sub> is to form CT complexes between TiO<sub>2</sub> and the surface adsorbate (ligand), neither of which absorbs visible light.<sup>210,220,221</sup> This CT-complex-mediated visible light sensitization operates by a mechanism that is different from the aforementioned dye sensitization. In the CT-sensitization, the electron is photo-excited directly from the ground state (HOMO level) of the adsorbate (ligand) (without involving the excited state of the adsorbate) to the semiconductor CB with mainly metal orbital characters (so named as ligand-to-metal charge transfer, LMCT) (Fig. 13a), whereas the dye sensitization is mediated through the excited dye state. Many examples of CT-complex formation on the TiO<sub>2</sub> surface have been reported. The TiO<sub>2</sub>-catechol complex is a classical example of CT-complexation. A theoretical calculation study provided evidence that the visible light absorption is caused by the LMCT and the excited state of catechol is not significantly involved in the photoinjection process.<sup>208</sup> 8-Hydroxyorthoquinoline and 1,1-binaphthalene-2,2-diol also form complexes with the TiO<sub>2</sub> surface, absorbing visible light and exhibiting some activity for H<sub>2</sub> production under visible light.<sup>202,203</sup> Many organic compounds with phenolic or carboxylic groups (e.g., chlorophenol<sup>205</sup> and calixarene<sup>206</sup>) are able to make LMCT-complexes with the TiO<sub>2</sub> surface for visible light absorption. Upon coupling with TiO<sub>2</sub>, the relatively electron-rich compounds with linker groups (e.g., enediol, carboxylate, nitrile, and alcohol) exhibit a LMCT band in the visible region, whereas the less electron-rich compounds (e.g., thiocyanate) display the band in the UV region.<sup>209</sup> The HOMO level of the adsorbate is also very important in determining the active light absorption range of the LMCT system. If there is strong coupling between the molecular orbital (HOMO) of the adsorbate and the energy band of the semiconductor, a new absorption band could appear that is absent in either the adsorbate or the semiconductor alone.

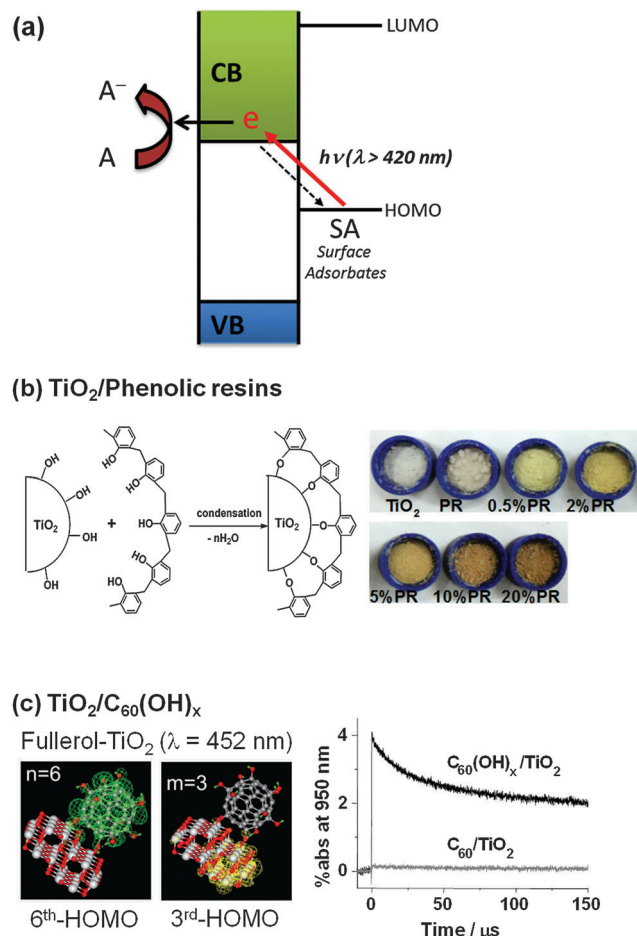


**Fig. 13** Schematic illustration of (a) the ligand-to-metal charge transfer (LMCT) mechanism, (b) LMCT by phenolic resins, and (c) LMCT with the adsorbates of C<sub>60</sub>(OH)<sub>x</sub>. (b) Reproduced from ref. 211 with permission from The Royal Society of Chemistry. (c) Reprinted with permission from ref. 207 (Copyright 2009 Wiley-VCH Verlag GmbH & Co. KGaA, Weinheim).

Incidentally, the fact that pure TiO<sub>2</sub> sometimes exhibits visible light activity for the degradation of organic substrates that do not absorb visible light at all can be ascribed to the LMCT mechanism. For example, phenol and 4-CP can be successfully degraded with the production of chloride ions or/and CO<sub>2</sub> in the visible light illuminated ( $\lambda > 420$  nm) aqueous suspension of pure TiO<sub>2</sub> although neither TiO<sub>2</sub> nor phenolic compounds absorb visible light.<sup>205</sup> This is because the phenolic compound adsorbed on TiO<sub>2</sub> (though very weakly) can inject an electron to the TiO<sub>2</sub> CB through LMCT with oxidizing itself.

LMCT sensitization with relatively cheap and commonly used compounds is also noteworthy. For example, ethylenediaminetetraacetate (EDTA) and formate that are widely utilized as electron donors in photochemical conversion systems can induce the LMCT-sensitization by forming surface complexes. The complexation of EDTA (or formate) on TiO<sub>2</sub> induces visible light absorption up to ~550 nm and exhibits a significant visible light activity for both the reductive conversion of Cr(vi) → Cr(III) and the production of H<sub>2</sub> from water.<sup>204</sup> Glucose that is also commonly employed as an electron donor in

photocatalysis can also form a LMCT complex on the TiO<sub>2</sub> surface.<sup>222</sup> The TiO<sub>2</sub>-glucose LMCT complex absorbs visible light significantly (up to 600 nm) and exhibits visible light activity for the photoconversion of Cr(vi) to Cr(III) and the production of H<sub>2</sub>O<sub>2</sub> via O<sub>2</sub> reduction. Hydrogen peroxide (H<sub>2</sub>O<sub>2</sub>) that is widely employed as an auxiliary oxidant in the TiO<sub>2</sub>/UV process can also form an LMCT complex on the TiO<sub>2</sub> surface but it is unstable and rapidly decomposes under visible light with the generation of an OH radical.<sup>84</sup> Although most LMCT sensitization systems are based on the chemisorbed adsorbates, the LMCT sensitization phenomenon can be observed even with physisorbed adsorbates in some cases. For instance, pure polycyclic arenes (chrysene, anthracene, pyrene and benzo[a]pyrene) can form LMCT complexes with the dry surface of TiO<sub>2</sub> (absence of adsorbed water molecules), and the resulting colored arene-TiO<sub>2</sub> complex could be reversibly bleached by desorbing the arenes without degrading the arene compounds.<sup>85</sup> A physical mixture of TiO<sub>2</sub> and non-ionic surfactants with polyoxyethylene groups (Brij series) that do not absorb visible light at all by themselves is another example of physisorbed LMCT.<sup>223</sup> The suspension of surfactant/TiO<sub>2</sub> showed a weak and broad absorption band in the visible light region (320–500 nm) and the visible light-induced electron transfer initiated on the surfactant/TiO<sub>2</sub> reductively transformed CCl<sub>4</sub> into Cl<sup>-</sup> and CO<sub>2</sub> or Cr(vi) into Cr(III). Considering the above examples, it seems that the visible light induced charge transfer occurring directly between the surface adsorbate and the semiconductor is quite ubiquitous as long as the HOMO level of the adsorbate lies below the CB edge level. However, the degree of charge transfer interaction is usually very weak and often negligible unless the interfacial orbital coupling is strong.

The LMCT sensitization phenomenon can be actively employed as a basis of the development of visible light active photocatalysts. For example, a linear-structured novolac type phenolic resin (PR) was shown to be successfully grafted onto the TiO<sub>2</sub> surface by simply dispersing the PR and TiO<sub>2</sub> powders in acetone (Fig. 13b).<sup>211</sup> The PR/TiO<sub>2</sub> exhibited a yellowish and brownish color (depending on the PR loading) and was found to be active for the evolution of H<sub>2</sub> from water and the degradation of 4-CP under visible light ( $\lambda > 420$  nm). The direct HOMO (~6.6 eV)-LUMO (~3.1 eV) excitation of PR requires 3.5 eV, which cannot be induced by visible light, but the LMCT between the PR HOMO and the TiO<sub>2</sub> CB is enabled by visible light photons of ca. 2.2 eV (<560 nm). The PR as a sensitizer of TiO<sub>2</sub> has the following advantages: (1) the synthesis process is easy, fast, and mild, (2) it is insoluble and stable in water, (3) it rapidly forms a surface complex without the need of additional linkage groups, and (4) it is much cheaper than organometallic dye sensitizers. Another LMCT-type visible light photocatalyst was developed by anchoring fullerol (C<sub>60</sub>(OH)<sub>x</sub>) on the surface of TiO<sub>2</sub> (Fig. 13c).<sup>207</sup> In contrast to fullerene (C<sub>60</sub>), fullerol adsorbs well on TiO<sub>2</sub> at pH 3 via monodentate and/or multidentate hydroxyl group complexation. The adsorbed fullerol activates TiO<sub>2</sub> under visible light irradiation through the CT-sensitization mechanism, which is insignificant in the fullerene/TiO<sub>2</sub> system. Fullerol/TiO<sub>2</sub> exhibits significant visible photocatalytic activity for not only the redox conversion of organic and inorganic



substrates (4-CP,  $\text{I}^-$ , and Cr(vi)), but also  $\text{H}_2$  evolution from water. The surface complexation of fullerol/TiO<sub>2</sub> induces a visible absorption band around 400–500 nm, which is extinguished when the adsorption of fullerol is inhibited. Transient absorption spectroscopic measurements revealed an absorption spectrum ascribed to the fullerol radical cation (fullerol•<sup>+</sup>), the generation of which should be accompanied by the proposed CT. Theoretical calculations regarding the absorption spectra for the “TiO<sub>2</sub> cluster+fullerol” model also confirmed the proposed CT, which involves the excitation from the HOMO (fullerol) to the LUMO (TiO<sub>2</sub> cluster) as the origin of the visible-light absorption of fullerol/TiO<sub>2</sub>.

## 5. Dual purpose photocatalysis for simultaneous energy and environmental applications

The photocatalytic conversion processes are carried out under different experimental conditions depending on their applications. The photocatalysis for the degradation of pollutants is initiated by single electron transfer resulting in the generation of reactive radical species, and therefore this process is usually carried out in the presence of dissolved O<sub>2</sub> (aerated condition). The dioxygen is needed not only as an electron acceptor that scavenges the CB electrons but also as a precursor of ROS and a reactant for mineralization.<sup>96,126,127,224</sup> Therefore, the photocatalytic degradation and mineralization of organic substrates

do not proceed in the absence of O<sub>2</sub>. On the other hand, the photocatalysis for solar fuel synthesis such as H<sub>2</sub> production is mediated by a multi-electron transfer process and is carried out in the absence of O<sub>2</sub> (anoxic condition), the presence of which should compete with H<sub>2</sub>O (or protons) for CB electrons and reoxidize H<sub>2</sub> back to water. The presence of dioxygen hinders the photocatalytic production of H<sub>2</sub>. Therefore, the two photocatalytic systems have been practiced separately under different reaction conditions and any photocatalyst may not be optimized for both purposes. A good photocatalyst for the environmental cleanup may be poor for solar fuel synthesis, while an excellent photocatalyst for water splitting may be poor for environmental remediation purpose. It is quite challenging to achieve the two purposes in a single system of “dual-functional photocatalysis” (e.g., simultaneous production of H<sub>2</sub> and the degradation of pollutants in wastewater). To achieve this, photocatalysts should be able to oxidize organic substrates by utilizing proton or water (not O<sub>2</sub>) as an electron acceptor while producing hydrogen at the same time. The successful development of this concept would realize the photocatalytic water treatment that removes unwanted organic pollutants and recovers H<sub>2</sub> as an energy resource at the same time. Although this system is conceptually identical to widely investigated sacrificial photocatalytic systems for H<sub>2</sub> production, which employ excess amounts of good electron donors (e.g., organic acids, alcohols, and sulfides/sulfites),<sup>225–228</sup> the challenge lies in the development of photocatalysts that can utilize low concentration organic contaminants as electron donors for H<sub>2</sub> production. If organic pollutants can be

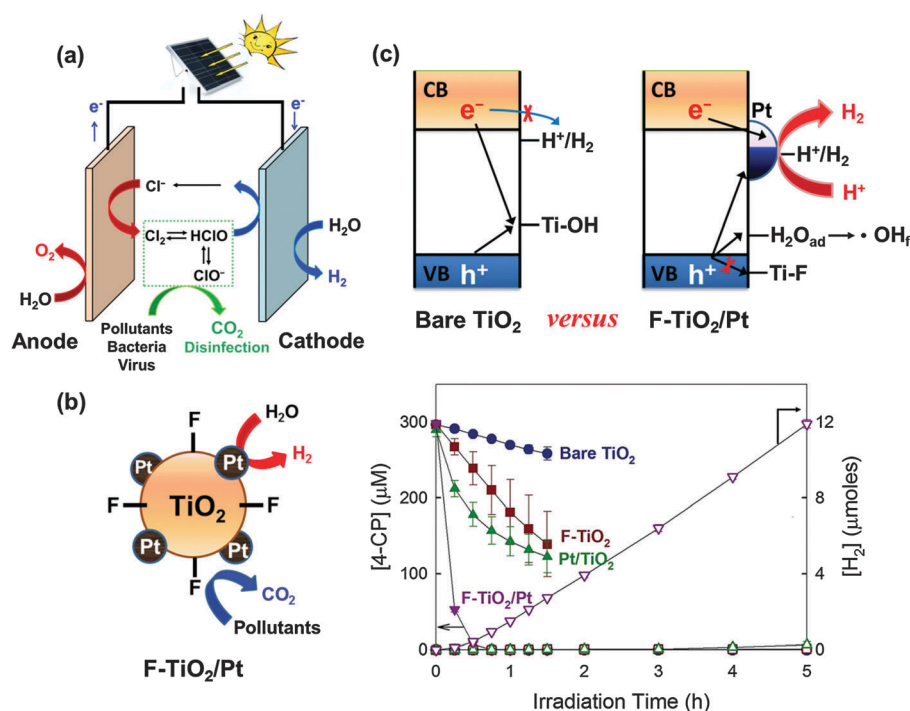


Fig. 14 (a) Applications of charge transfer to the energy-water nexus. The photovoltaic-assisted electrochemical system can effectively remediate water pollutants and deactivate bacteria/virus in the presence of chloride at the anode, while chemical fuels (e.g., H<sub>2</sub>) can be produced at the cathode. (b and c) This dual function of the semiconductor can be achieved in particulate (suspension) systems (e.g., F-TiO<sub>2</sub>/Pt) without power assistance. Reproduced from ref. 250 with permission from The Royal Society of Chemistry.

used as electron donors for H<sub>2</sub> production, the overall photocatalytic process can be cost-effective. The development of photocatalytic systems that combine wastewater treatment and H<sub>2</sub> production is promising because a variety of organic pollutants found in wastewaters may serve as precursors for H<sub>2</sub> in solar photocatalysis.

Many electrochemical and PEC studies have investigated the simultaneous production of energy (*e.g.*, H<sub>2</sub> and electricity) and the degradation of organic pollutants (*e.g.*, phenolic compounds, dyes, organic acids, actual wastewater, and urea/urine).<sup>229–234</sup> They have used either external electrical energy or photovoltaics (Fig. 14a). Conceptually, the dual functional process occurring on (suspended) TiO<sub>2</sub> particles is similar to the case of a (photo)-electrochemical system. However, since external electric power cannot be applied to the slurry system, the efficiency of the charge pair separation in a single TiO<sub>2</sub> particle is low.<sup>235</sup> The functional photocatalysis usually needs the presence of co-catalysts (*e.g.*, Pt for hydrogen evolution reaction and RuO<sub>2</sub> for oxygen evolution reaction) that are deposited on the TiO<sub>2</sub> surface.<sup>236</sup>

Recently, TiO<sub>2</sub> the surface of which is modified with both fluoride (or phosphate) and platinum nanoparticle (F-TiO<sub>2</sub>/Pt or P-TiO<sub>2</sub>/Pt) has been successfully demonstrated for the dual function photocatalysis: simultaneous degradation of organic compounds and H<sub>2</sub> production under a solar simulating condition ( $\lambda > 320$  nm) (Fig. 14b).<sup>76,79,80</sup> Surface fluorination (or phosphation) replaces the surface hydroxyl groups on TiO<sub>2</sub>, favoring the formation of unbound OH radicals ( $\bullet\text{OH}_f$ ) instead of surface-bound OH radicals ( $\geq\text{Ti-OH}^\bullet$ ) (Fig. 14c).<sup>62,65,75,77,78,237</sup> Since the surface-bound OH radicals (or surface-trapped holes) serve as a site of recombination with CB electrons, the fluoride substitution reduces the chance of recombination of CB electrons with the surface trapped holes on TiO<sub>2</sub> particles. Meanwhile, surface platinization accelerates the electron transfer and further retards the charge pair recombination, thereby enhancing H<sub>2</sub> production significantly.<sup>23,32,37,85,99,114,238</sup> With these catalysts, the degradation of 4-CP and urea can be accompanied by the concurrent production of H<sub>2</sub> (Fig. 14b). The synergistic effect greatly depends on the type of metal (Pt, Pd, Au, Ag, Cu, or Ni) and pH. The activity of F-TiO<sub>2</sub>/Pt gradually decreases with increasing pH, owing to the desorption of fluoride from the TiO<sub>2</sub> surface. On the other hand, P-TiO<sub>2</sub>/Pt maintains the activity over a wide pH range because of the stability of the adsorbed phosphate, making the catalyst a more practical dual-function photocatalyst. Recently, the F-TiO<sub>2</sub>/Pt catalyst was further modified by the third component, graphene oxide (GO), to enhance the dual-functional photocatalytic activity.<sup>239</sup> GO on TiO<sub>2</sub> attracts electrons and facilitates the electron transfer to Pt. The positive effect of GO on the dual photocatalytic activity was observed only when Pt and surface fluoride are co-present. The photocatalytic activity of Pt/GO/TiO<sub>2</sub>-F (ternary system) for the simultaneous H<sub>2</sub> production accompanied with the degradation of 4-CP was much higher than that of any binary-component photocatalysts, which confirmed the synergic role of the three components (*i.e.*, GO, Pt, F).

## 6. Concluding remarks

Most semiconductor metal oxides including titania have limited photoactivity because of rapid charge recombination. The surface modification of semiconductor photocatalysts is a facile and soft method without reconstructing the solid lattice structure and has been widely attempted to improve the photocatalytic activity under UV and/or visible light irradiation. The modified surface of semiconductor critically influences the photo-induced CT behaviors at the interfacial region (particle/solution, particle/air, and particle/particle). Therefore, it is essential to understand how the modified surface properties control the primary factors involved in the overall photocatalysis. The photogenerated charge carriers follow various pathways which include recombination, trapping (at surface and bulk defect sites), transfer to a reservoir phase (*e.g.*, Pt, graphene), transfer to bordering particles (of the same or different kind), and transfer to electron acceptors/donors in the electrolyte. For desirable photocatalytic reactions, the eventual transfer to electron acceptors or donors (*i.e.*, target substrate) should be maximized, which can be controlled by modifying the surface properties. The effects of a specific modification method depend on many parameters and are specific to the kind of substrates, the characteristics of target reactions, and the experimental conditions. For example, a modified semiconductor optimized for a single-CT may not be good for a multiple-CT system (*and vice versa*). Therefore, it is usually not possible to generalize the effects of a specific modification method: even the same modified semiconductor may exhibit either a positive or a negative effect depending on the nature of the target photocatalytic conversion system. This implies that finding out “the best modification method” out of numerous possible ways of semiconductor modifications is not very meaningful. Each modification method and its related effects can be clearly defined only for a specific photocatalytic system. For example, it is not difficult to find out the published articles which claim to have developed a very efficient photocatalyst (hybrid or modified) based on a dye-discoloration measurement with an assumption that the particular photocatalyst would also be good for other photocatalytic conversion systems in general, which is actually not. The result could be different for other photocatalytic systems and even for a different dye.<sup>240</sup> Therefore, the modification method of semiconductor photocatalysts should be cautiously chosen or designed on the basis of clear understanding of the characteristics of the target reaction. The dual-function photocatalysis, for example, aims to achieve the single CT for the pollutant oxidation part but the multiple-CT for H<sub>2</sub> production part on the contrary, which is to control the transfer of holes and electrons in semiconductor particles in different ways. The development of appropriate modification methods to selectively control the CT behavior may realize such a goal.

## Acknowledgements

This research was financially supported by the Global Research Laboratory (GRL) Program (No. NRF-2014K1A1A2041044), the Global Frontier R&D Program on Center for Multiscale Energy



System (2011-0031571), and KCAP (Sogang Univ.) (No. 2009-0093880), which were funded by the Korea Government (MSIP) through the National Research Foundation (NRF). H. P. is grateful to the Global Research Network Program (NRF-2014S1A2A2027802) for financial support.

## References

- 1 N. Serpone and E. Pelizzetti, *Photocatalysis: Fundamentals and Applications*, Wiley, New York, 1989.
- 2 C. A. Grimes, O. K. Varghese and S. Ranjan, *Light, Water, Hydrogen: The Solar Generation of Hydrogen by Water Photoelectrolysis*, Springer, New York, 2008.
- 3 R. Van de Krol and M. Gratzel, *Photoelectrochemical Hydrogen Production*, Springer, New York, 2012.
- 4 M. R. Hoffmann, S. T. Martin, W. Choi and D. W. Bahnemann, *Chem. Rev.*, 1995, **95**, 69–96.
- 5 A. Fujishima, X. T. Zhang and D. A. Tryk, *Surf. Sci. Rep.*, 2008, **63**, 515–582.
- 6 M. J. Esswein and D. G. Nocera, *Chem. Rev.*, 2007, **107**, 4022–4047.
- 7 W. Choi, *Catal. Surv. Asia*, 2006, **10**, 16–28.
- 8 H. Park, Y. Park, Y. Kim and W. Choi, *J. Photochem. Photobiol. C*, 2012, **15**, 1–20.
- 9 *On Solar Hydrogen & Nanotechnology*, ed. L. Vayssières, Wiley, Singapore, 2009.
- 10 J. Lee, J. Kim and W. Choi, in *Aquatic Redox Chemistry*, ed. P. G. Tratnyek, T. J. Grundl and S. B. Haderlein, American Chemical Society, Washington, 2011.
- 11 S. Licht, in *Encyclopedia of Electrochemistry*, ed. A. J. Bard and M. Stratmann, Wiley-VCH, Weinheim, 2002.
- 12 N. Serpone, *J. Phys. Chem. B*, 2006, **110**, 24287–24293.
- 13 P. V. Kamat, *J. Phys. Chem. B*, 2002, **106**, 7729–7744.
- 14 T. L. Thompson and J. T. Yates, Jr., *J. Phys. Chem. B*, 2005, **109**, 18230–18236.
- 15 G. Hodes, *J. Phys. Chem. C*, 2008, **112**, 17778–17787.
- 16 T. Tachikawa, M. Fujitsuka and T. Majima, *J. Phys. Chem. C*, 2007, **111**, 5259–5275.
- 17 K. Maeda and K. Domen, *J. Phys. Chem. Lett.*, 2010, **1**, 2655–2661.
- 18 J. A. Turner, *Science*, 1999, **285**, 687–689.
- 19 U. Kang and H. Park, *Appl. Catal. B*, 2013, **140–141**, 233–240.
- 20 T. H. Jeon, S. K. Choi, H. W. Jeong, S. Kim and H. Park, *J. Electrochem. Sci. Technol.*, 2011, **2**, 187–192.
- 21 M. Tabata, K. Maeda, M. Higashi, D. L. Lu, T. Takata, R. Abe and K. Domen, *Langmuir*, 2010, **26**, 9161–9165.
- 22 H. W. Jeong, S.-Y. Choi, S. H. Hong, S. K. Lim, D. S. Han, A. Abdel-Wahab and H. Park, *J. Phys. Chem. C*, 2014, **118**, 21331–21338.
- 23 J. Kim, C. W. Lee and W. Choi, *Environ. Sci. Technol.*, 2010, **44**, 6849–6854.
- 24 J. Kim and W. Choi, *Environ. Sci. Technol.*, 2011, **45**, 3183–3184.
- 25 H.-i. Kim, J. Kim, W. Kim and W. Choi, *J. Phys. Chem. C*, 2011, **115**, 9797–9805.
- 26 H. Park, A. Bak, T. H. Jeon, S. Kim and W. Choi, *Appl. Catal. B*, 2012, **115–116**, 74–80.
- 27 C. Tagusagawa, A. Takagaki, A. Iguchi, K. Takanabe, J. N. Kondo, K. Ebitani, T. Tatsumi and K. Domen, *Chem. Mater.*, 2010, **22**, 3072–3078.
- 28 A. Bak, W. Choi and H. Park, *Appl. Catal. B*, 2011, **110**, 207–215.
- 29 T. H. Jeon, W. Choi and H. Park, *Phys. Chem. Chem. Phys.*, 2011, **13**, 21392–21401.
- 30 M. Yoshida, T. Hirai, K. Maeda, N. Saito, J. Kubota, H. Kobayashi, Y. Inoue and K. Domen, *J. Phys. Chem. C*, 2010, **114**, 15510–15515.
- 31 D. Yokoyama, T. Minegishi, K. Maeda, M. Katayama, J. Kubota, A. Yamada, M. Konagai and K. Domen, *Electrochim. Commun.*, 2010, **12**, 851–853.
- 32 H. Park, W. Choi and M. R. Hoffmann, *J. Mater. Chem.*, 2008, **18**, 2379–2385.
- 33 Y. K. Kim and H. Park, *Energy Environ. Sci.*, 2011, **4**, 685–694.
- 34 G. Khan, S. K. Choi, S. Kim, S. K. Lim, J. S. Jang and H. Park, *Appl. Catal. B*, 2013, **142–143**, 647–653.
- 35 Y. Kim and H. Park, *Appl. Catal. B*, 2012, **125**, 530–537.
- 36 U. Kang, S. K. Choi, D. J. Ham, S. M. Ji, W. Choi, D. S. Han, A. Abdel-Wahab and H. Park, *Energy Environ. Sci.*, 2015, **8**, 2638–2643.
- 37 H. Park and W. Choi, *J. Phys. Chem. B*, 2003, **107**, 3885–3890.
- 38 K. Maeda, M. Higashi, D. L. Lu, R. Abe and K. Domen, *J. Am. Chem. Soc.*, 2010, **132**, 5858–5868.
- 39 J. A. Seabold and K. S. Choi, *Chem. Mater.*, 2011, **23**, 1105–1112.
- 40 Y. Surendranath, M. Dinca and D. G. Nocera, *J. Am. Chem. Soc.*, 2009, **131**, 2615–2620.
- 41 S. K. Choi, W. Choi and H. Park, *Phys. Chem. Chem. Phys.*, 2013, **15**, 6499–6507.
- 42 D. K. Bediako, B. Lassalle-Kaiser, Y. Surendranath, J. Yano, V. K. Yachandra and D. G. Nocera, *J. Am. Chem. Soc.*, 2012, **134**, 6801–6809.
- 43 C. Tagusagawa, A. Takagaki, K. Takanabe, K. Ebitani, S. Hayashi and K. Domen, *J. Catal.*, 2010, **270**, 206–212.
- 44 S. J. Li, Z. C. Ma, J. Zhang, Y. S. Wu and Y. M. Gong, *Catal. Today*, 2008, **139**, 109–112.
- 45 A. Kudo and Y. Miseki, *Chem. Soc. Rev.*, 2009, **38**, 253–278.
- 46 E. R. Carraway, A. J. Hoffman and M. R. Hoffmann, *Environ. Sci. Technol.*, 1994, **28**, 786–793.
- 47 C. Richard, *J. Photochem. Photobiol. A*, 1993, **72**, 179–182.
- 48 Y. Mao, C. Schoneich and K. D. Asmus, *J. Phys. Chem.*, 1991, **95**, 10080–10089.
- 49 R. B. Draper and M. A. Fox, *Langmuir*, 1990, **6**, 1396–1402.
- 50 S. Kim and W. Choi, *Environ. Sci. Technol.*, 2002, **36**, 2019–2025.
- 51 M. C. Lee and W. Choi, *J. Phys. Chem. B*, 2002, **106**, 11818–11822.
- 52 S. Chen and L.-W. Wang, *Chem. Mater.*, 2012, **24**, 3659–3666.
- 53 W. Choi, A. Termin and M. R. Hoffmann, *J. Phys. Chem.*, 1994, **98**, 13669–13679.
- 54 W. Choi, A. Termin and M. R. Hoffmann, *Angew. Chem. Int. Ed. Engl.*, 1994, **33**, 1091–1092.



- 55 M. Mrowetz, W. Balcerski, A. J. Colussi and M. R. Hoffmann, *J. Phys. Chem. B*, 2004, **108**, 17269–17273.
- 56 S. Kim, S. J. Hwang and W. Choi, *J. Phys. Chem. B*, 2005, **109**, 24260–24267.
- 57 Y. Park, W. Kim, H. Park, T. Tachikawa, T. Majima and W. Choi, *Appl. Catal., B*, 2009, **91**, 355–361.
- 58 W. Kim, T. Tachikawa, H. Kim, N. Lakshminarasimhan, P. Murugan, H. Park, T. Majima and W. Choi, *Appl. Catal., B*, 2014, **147**, 642–650.
- 59 W. Choi, S. J. Hong, Y. S. Chang and Y. Cho, *Environ. Sci. Technol.*, 2000, **34**, 4810–4815.
- 60 C. X. Zhang, T. L. Sun and X. M. Sun, *Environ. Sci. Technol.*, 2011, **45**, 4756–4762.
- 61 H. Park and W. Choi, *J. Phys. Chem. B*, 2005, **109**, 11667–11674.
- 62 M. S. Vohra, S. Kim and W. Choi, *J. Photochem. Photobiol., A*, 2003, **160**, 55–60.
- 63 G. Zhang, W. Choi, S. H. Kim and S. B. Hong, *J. Hazard. Mater.*, 2011, **188**, 198–205.
- 64 P. Chin, C. S. Grant and D. F. Ollis, *Appl. Catal., B*, 2009, **87**, 220–229.
- 65 J. S. Park and W. Choi, *Langmuir*, 2004, **20**, 11523–11527.
- 66 H. Haick and Y. Paz, *J. Phys. Chem. B*, 2001, **105**, 3045–3051.
- 67 S. K. Lee, S. McIntyre and A. Mills, *J. Photochem. Photobiol., A*, 2004, **162**, 203–206.
- 68 J. S. Park and W. Choi, *Chem. Lett.*, 2005, **34**, 1630–1631.
- 69 T. Tatsuma, W. Kubo and A. Fujishima, *Langmuir*, 2002, **18**, 9632–9634.
- 70 T. Tatsuma, S. Tachibana and A. Fujishima, *J. Phys. Chem. B*, 2001, **105**, 6987–6992.
- 71 T. Tatsuma, S. Tachibana, T. Miwa, D. A. Tryk and A. Fujishima, *J. Phys. Chem. B*, 1999, **103**, 8033–8035.
- 72 S. M. Cho and W. Choi, *J. Photochem. Photobiol., A*, 2001, **143**, 221–228.
- 73 P. Chin, G. W. Roberts and D. F. Ollis, *Ind. Eng. Chem. Res.*, 2007, **46**, 7598–7604.
- 74 W. Kim, T. Tachikawa, G. Moon, T. Majima and W. Choi, *Angew. Chem., Int. Ed.*, 2014, **53**, 14036–14041.
- 75 H. Park and W. Choi, *J. Phys. Chem. B*, 2004, **108**, 4086–4093.
- 76 J. Kim and W. Choi, *Appl. Catal., B*, 2011, **106**, 39–45.
- 77 H. Kim and W. Choi, *Appl. Catal., B*, 2006, **69**, 127–132.
- 78 J. Kim, W. Choi and H. Park, *Res. Chem. Intermed.*, 2010, **36**, 127–140.
- 79 J. Kim, J. Lee and W. Choi, *Chem. Commun.*, 2008, 756–758.
- 80 J. Kim, D. Monllor-Satoca and W. Choi, *Energy Environ. Sci.*, 2012, **5**, 7647–7656.
- 81 C. Minero, G. Mariella, V. Maurino and E. Pelizzetti, *Langmuir*, 2000, **16**, 2632–2641.
- 82 V. Maurino, C. Minero, G. Mariella and E. Pelizzetti, *Chem. Commun.*, 2005, 2627–2629.
- 83 M. Mrowetz and E. Selli, *Phys. Chem. Chem. Phys.*, 2005, **7**, 1100–1102.
- 84 T. Ohno, F. Tanigawa, K. Fujihara, S. Izumi and M. Matsumura, *J. Photochem. Photobiol., A*, 1998, **118**, 41–44.
- 85 H. Park, J. Lee and W. Choi, *Catal. Today*, 2006, **111**, 259–265.
- 86 R. Abe, M. Higashi and K. Domen, *J. Am. Chem. Soc.*, 2010, **132**, 11828–11829.
- 87 S. S. K. Ma, T. Hisatomi, K. Maeda, Y. Moriya and K. Domen, *J. Am. Chem. Soc.*, 2012, **134**, 19993–19996.
- 88 H. Kim, H.-Y. Yoo, S. Hong, S. Lee, B.-S. Park, H. Park, C. Lee and J. Lee, *Appl. Catal., B*, 2015, **162**, 515–523.
- 89 D. F. Evans and M. W. Upton, *J. Chem. Soc., Dalton Trans.*, 1985, 1141–1145.
- 90 S. T. Martin, A. T. Lee and M. R. Hoffmann, *Environ. Sci. Technol.*, 1995, **29**, 2567–2573.
- 91 E. Pelizzetti, V. Carlin, C. Minero and M. Gratzel, *New J. Chem.*, 1991, **15**, 351–359.
- 92 W. V. Steele and E. H. Appelman, *J. Chem. Thermodyn.*, 1982, **14**, 337–344.
- 93 R. R. Ozer and J. L. Ferry, *Environ. Sci. Technol.*, 2001, **35**, 3242–3246.
- 94 I. A. Weinstock, *Chem. Rev.*, 1998, **98**, 113–170.
- 95 J. Lee, J. Kim and W. Choi, *Environ. Sci. Technol.*, 2007, **41**, 3335–3340.
- 96 J. Ryu and W. Choi, *Environ. Sci. Technol.*, 2006, **40**, 7034–7039.
- 97 Y. Cho, W. Choi, C. H. Lee, T. Hyeon and H. I. Lee, *Environ. Sci. Technol.*, 2001, **35**, 966–970.
- 98 E. Bae and W. Choi, *Environ. Sci. Technol.*, 2002, **37**, 147–152.
- 99 S. Kim and W. Choi, *J. Phys. Chem. B*, 2002, **106**, 13311–13317.
- 100 C. D. Vecitis, H. Park, J. Cheng, B. T. Mader and M. R. Hoffmann, *Front. Environ. Sci. Eng. China*, 2009, **3**, 129–151.
- 101 H. Park, C. D. Vecitis, J. Cheng, W. Choi, B. T. Mader and M. R. Hoffmann, *J. Phys. Chem. A*, 2009, **113**, 690–696.
- 102 E. Szajdzinska-Pietek and J. L. Gebicki, *Res. Chem. Intermed.*, 2000, **26**, 897–912.
- 103 H. Park, C. D. Vecitis, J. Cheng, N. F. Dalleska, B. T. Mader and M. R. Hoffmann, *Photochem. Photobiol. Sci.*, 2011, **10**, 1945–1953.
- 104 H. Kyung, J. Lee and W. Choi, *Environ. Sci. Technol.*, 2005, **39**, 2376–2382.
- 105 S. Kim and H. Park, *RSC Adv.*, 2013, **3**, 17551–17558.
- 106 W. Choi and M. R. Hoffmann, *Environ. Sci. Technol.*, 1995, **29**, 1646–1654.
- 107 W. Choi and M. R. Hoffmann, *Environ. Sci. Technol.*, 1997, **31**, 89–95.
- 108 B. Kraeutler and A. J. Bard, *J. Am. Chem. Soc.*, 1978, **100**, 4317–4318.
- 109 M. Jakob, H. Levanon and P. V. Kamat, *Nano Lett.*, 2003, **3**, 353–358.
- 110 W. Choi, J. Lee, S. Kim, S. Hwang, M. C. Lee and T. K. Lee, *J. Ind. Eng. Chem.*, 2003, **9**, 96–101.
- 111 J. Lee, W. Choi and J. Yoon, *Environ. Sci. Technol.*, 2005, **39**, 6800–6807.
- 112 I. Mikami, S. Aoki and Y. Miura, *Chem. Lett.*, 2010, **39**, 704–705.
- 113 L. A. Pretzer, P. J. Carlson and J. E. Boyd, *J. Photochem. Photobiol., A*, 2008, **200**, 246–253.



- 114 J. Lee and W. Choi, *Environ. Sci. Technol.*, 2004, **38**, 4026–4033.
- 115 J. Lee and W. Choi, *J. Phys. Chem. B*, 2005, **109**, 7399–7406.
- 116 J. Lee, H. Park and W. Choi, *Environ. Sci. Technol.*, 2002, **36**, 5462–5468.
- 117 W. Zhao, C. Chen, X. Li, J. Zhao, H. Hidaka and N. Serpone, *J. Phys. Chem. B*, 2002, **106**, 5022–5028.
- 118 N. Z. Muradov, *Sol. Energy*, 1994, **52**, 283–288.
- 119 D. Hufschmidt, D. Bahnemann, J. J. Testa, C. A. Emilio and M. I. Litter, *J. Photochem. Photobiol. A*, 2002, **148**, 223–231.
- 120 B. Sun, V. Vorontsov and P. G. Smirniotis, *Langmuir*, 2003, **19**, 3151–3156.
- 121 M. Trillas, J. Peral and X. Domenech, *Appl. Catal. B*, 1995, **5**, 377–387.
- 122 B. H. J. Bielski, D. E. Cabelli, R. L. Arudi and A. B. Ross, *J. Phys. Chem. B*, 1985, **14**, 1041–1100.
- 123 A. J. Cowan, J. W. Tang, W. H. Leng, J. R. Durrant and D. R. Klug, *J. Phys. Chem. C*, 2010, **114**, 4208–4214.
- 124 H. Gerischer and A. Heller, *J. Phys. Chem.*, 1991, **95**, 5261–5267.
- 125 W. Choi, J. Yeo, J. Ryu, T. Tachikawa and T. Majima, *Environ. Sci. Technol.*, 2010, **44**, 9099–9104.
- 126 J. Ryu and W. Choi, *Environ. Sci. Technol.*, 2004, **38**, 2928–2933.
- 127 J. Ryu and W. Choi, *Environ. Sci. Technol.*, 2007, **41**, 6313–6314.
- 128 D. Monllor-Satoca, T. Tachikawa, T. Majima and W. Choi, *Environ. Sci. Technol.*, 2011, **45**, 2030–2031.
- 129 D. Monllor-Satoca, R. Gomez and W. Choi, *Environ. Sci. Technol.*, 2012, **46**, 5519–5527.
- 130 H. Lee and W. Choi, *Environ. Sci. Technol.*, 2002, **36**, 3872–3878.
- 131 C. Kormann, D. W. Bahnemann and M. R. Hoffmann, *Environ. Sci. Technol.*, 1988, **22**, 798–806.
- 132 X. Z. Li, C. C. Chen and J. C. Zhao, *Langmuir*, 2001, **17**, 4118–4122.
- 133 M. Teranishi, S. Naya and H. Tada, *J. Am. Chem. Soc.*, 2010, **132**, 7850–7851.
- 134 J. Yi, C. Bahrini, C. Schoemaecker, C. Fittschen and W. Choi, *J. Phys. Chem. C*, 2012, **116**, 10090–10097.
- 135 N. M. Dimitrijevic, B. K. Vijayan, O. G. Poluektov, T. Rajh, K. A. Gray, H. Y. He and P. Zapol, *J. Am. Chem. Soc.*, 2011, **133**, 3964–3971.
- 136 E. Fujita, *Coord. Chem. Rev.*, 1999, **185–186**, 373–384.
- 137 T. Yui, A. Kan, C. Saitoh, K. Koike, T. Ibusuki and O. Ishitani, *ACS Appl. Mater. Interfaces*, 2011, **3**, 2594–2600.
- 138 S. K. Choi, U. Kang, S. Lee, D. J. Ham, S. M. Ji and H. Park, *Adv. Energy Mater.*, 2014, **4**, 1301614.
- 139 H. Park, H.-H. Qu, A. J. Colussi and M. R. Hoffmann, *J. Phys. Chem. A*, 2015, **119**, 4658–4666.
- 140 J. R. Bolton, S. J. Strickler and J. S. Connolly, *Nature*, 1985, **316**, 495–500.
- 141 J. Greeley, T. F. Jaramillo, J. Bonde, I. B. Chorkendorff and J. K. Norskov, *Nat. Mater.*, 2006, **5**, 909–913.
- 142 S. Trasatti, *J. Electroanal. Chem.*, 1972, **39**, 163–184.
- 143 T. Hisatomi, K. Miyazaki, K. Takanabe, K. Maeda, J. Kubota, Y. Sakata and K. Domen, *Chem. Phys. Lett.*, 2010, **486**, 144–146.
- 144 K. Maeda and K. Domen, *Chem. Mater.*, 2010, **22**, 612–623.
- 145 Y. Park, S. H. Kang and W. Choi, *Phys. Chem. Chem. Phys.*, 2011, **13**, 9425–9431.
- 146 R. Leary and A. Westwood, *Carbon*, 2011, **49**, 741–772.
- 147 G. H. Moon, Y. Park, W. Kim and W. Choi, *Carbon*, 2011, **49**, 3454–3462.
- 148 L.-L. Tan, S.-P. Chai and A. R. Mohamed, *ChemSusChem*, 2012, **5**, 1868–1882.
- 149 H.-i. Kim, G. H. Moon, D. Monllor-Satoca, Y. Park and W. Choi, *J. Phys. Chem. C*, 2012, **116**, 1535–1543.
- 150 G. Moon, D. Kim, H. Kim, A. D. Bokare and W. Choi, *Environ. Sci. Technol. Lett.*, 2014, **1**, 185–190.
- 151 G. Moon, W. Kim, A. D. Bokare, N. Sung and W. Choi, *Energy Environ. Sci.*, 2014, **7**, 4023–4028.
- 152 H.-i. Kim, S. Kim, J. Kang and W. Choi, *J. Catal.*, 2014, **309**, 49–57.
- 153 A. J. Hoffman, E. R. Carraway and M. R. Hoffmann, *Environ. Sci. Technol.*, 1994, **28**, 776–785.
- 154 W. Kim, T. Seok and W. Choi, *Energy Environ. Sci.*, 2012, **5**, 6066–6070.
- 155 A. J. Bard and M. A. Fox, *Acc. Chem. Res.*, 1995, **28**, 141–145.
- 156 Y. Park, K. J. McDonald and K.-S. Choi, *Chem. Soc. Rev.*, 2013, **42**, 2321–2337.
- 157 K. Sivula, F. Le Formal and M. Gratzel, *ChemSusChem*, 2011, **4**, 432–449.
- 158 F. X. Yin, K. Takanabe, M. Katayama, J. Kubota and K. Domen, *Electrochem. Commun.*, 2010, **12**, 1177–1179.
- 159 W. Kim, T. Tachikawa, D. Monllor-Satoca, H.-i. Kim, T. Majima and W. Choi, *Energy Environ. Sci.*, 2013, **6**, 3732–3739.
- 160 N. Lakshminarasimhan, W. Kim and W. Choi, *J. Phys. Chem. C*, 2008, **112**, 20451–20457.
- 161 Y. Park, W. Kim, D. Monllor-Satoca, T. Tachikawa, T. Majima and W. Choi, *J. Phys. Chem. Lett.*, 2013, **4**, 189–194.
- 162 N. Lakshminarasimhan, E. Bae and W. Choi, *J. Phys. Chem. C*, 2007, **111**, 15244–15250.
- 163 S. K. Choi, S. Kim, S. K. Lim and H. Park, *J. Phys. Chem. C*, 2010, **114**, 16475–16480.
- 164 T. H. Jeon, W. Choi and H. Park, *J. Phys. Chem. C*, 2011, **115**, 7134–7142.
- 165 J. S. Jang, S. H. Choi, H. Park, W. Choi and J. S. Lee, *J. Nanosci. Nanotechnol.*, 2006, **6**, 3642–3646.
- 166 S. K. Choi, S. Kim, J. Ryu, S. K. Lim and H. Park, *Photochem. Photobiol. Sci.*, 2012, **11**, 1437–1444.
- 167 H. W. Jeong, T. H. Jeon, J. S. Jang, W. Choi and H. Park, *J. Phys. Chem. C*, 2013, **117**, 9104–9112.
- 168 D. Zhao, C. C. Chen, C. L. Yu, W. H. Ma and J. C. Zhao, *J. Phys. Chem. C*, 2009, **113**, 13160–13165.
- 169 S. Biswas, M. F. Hossain, M. Shahjahan, K. Takahashi, T. Takahashi and A. Fujishima, *J. Vac. Sci. Technol. A*, 2009, **27**, 880–884.
- 170 W. Smith and Y. P. Zhao, *J. Phys. Chem. C*, 2008, **112**, 19635–19641.
- 171 L. X. Cao, F. J. Spiess, A. M. Huang, S. L. Suib, T. N. Obree, S. O. Hay and J. D. Freihaut, *J. Phys. Chem. B*, 1999, **103**, 2912–2917.



- 172 Y. Cao, X. T. Zhang, W. S. Yang, H. Du, Y. B. Bai, T. J. Li and J. N. Yao, *Chem. Mater.*, 2000, **12**, 3445–3448.
- 173 U. Scharf, M. Schramlmarth, A. Wokaun and A. Baiker, *J. Chem. Soc., Faraday Trans.*, 1991, **87**, 3299–3307.
- 174 J. H. Fang, J. W. Wu, X. M. Lu, Y. C. Shen and Z. H. Lu, *Chem. Phys. Lett.*, 1997, **270**, 145–151.
- 175 X. C. Shen, Z. L. Zhang, B. Zhou, J. Peng, M. Xie, M. Zhang and D. W. Pang, *Environ. Sci. Technol.*, 2008, **42**, 5049–5054.
- 176 H. Park, Y. K. Kim and W. Choi, *J. Phys. Chem. C*, 2011, **115**, 6141–6148.
- 177 J. S. Jang and H. Park, in *Materials and Processes for Solar Fuel Production*, ed. R. Subramanian, B. Viswanathan and J. S. Lee, Springer, New York, 2014.
- 178 H. Tada, A. Kokubu, M. Iwasaki and S. Ito, *Langmuir*, 2004, **20**, 4665–4670.
- 179 W. Smith and Y. P. Zhao, *Catal. Commun.*, 2009, **10**, 1117–1121.
- 180 B. Tryba, M. Piszez and A. W. Morawski, *Int. J. Photoenergy*, 2009, **2009**, 297319.
- 181 J. Papp, S. Soled, K. Dwight and A. Wold, *Chem. Mater.*, 1994, **6**, 496–500.
- 182 H. Park, K. Y. Kim and W. Choi, *Chem. Commun.*, 2001, 281–282.
- 183 H. Park, K. Y. Kim and W. Choi, *J. Phys. Chem. B*, 2002, **106**, 4775–4781.
- 184 R. Abe, H. Takami, N. Murakami and B. Ohtani, *J. Am. Chem. Soc.*, 2008, **130**, 7780–7781.
- 185 D. X. Shi, Y. Q. Feng and S. H. Zhong, *Catal. Today*, 2004, **98**, 505–509.
- 186 C. Y. Wang, H. M. Shang, T. Ying, T. S. Yuan and G. W. Zhang, *Sep. Purif. Technol.*, 2003, **32**, 357–362.
- 187 A. Kumar and A. K. Jain, *J. Photochem. Photobiol. A*, 2003, **156**, 207–218.
- 188 Y. Bessekhouad, N. Chaoui, M. Trzpits, N. Ghazzal, D. Robert and J. V. Weber, *J. Photochem. Photobiol. A*, 2006, **183**, 218–224.
- 189 H. B. Yin, Y. Wada, T. Kitamura, T. Sakata, H. Mori and S. Yanagida, *Chem. Lett.*, 2001, 334–335.
- 190 T. A. Khalyavka, E. I. Kapinus and T. I. Viktorova, *Pol. J. Chem.*, 2008, **82**, 107–112.
- 191 A. Kumar and A. K. Jain, *J. Mol. Catal. A: Chem.*, 2001, **165**, 265–273.
- 192 P. A. Sant and P. V. Kamat, *Phys. Chem. Chem. Phys.*, 2002, **4**, 198–203.
- 193 H. Matsumoto, T. Matsunaga, T. Sakata, H. Mori and H. Yoneyama, *Langmuir*, 1995, **11**, 4283–4287.
- 194 H. Tada, T. Mitsui, T. Kiyonaga, T. Akita and K. Tanaka, *Nat. Mater.*, 2006, **5**, 782–786.
- 195 N. Nishimura, B. Raphael, K. Maeda, L. Le Gendre, R. Abe, J. Kubota and K. Domen, *Thin Solid Films*, 2010, **518**, 5855–5859.
- 196 R. Ohnishi, M. Katayama, K. Takanabe, J. Kubota and K. Domen, *Electrochim. Acta*, 2010, **55**, 5393–5400.
- 197 T. Hisatomi, M. Otani, K. Nakajima, K. Teramura, Y. Kako, D. L. Lu, T. Takata, J. N. Kondo and K. Domen, *Chem. Mater.*, 2010, **22**, 3854–3861.
- 198 M. Tabata, K. Maeda, T. Ishihara, T. Minegishi, T. Takata and K. Domen, *J. Phys. Chem. C*, 2010, **114**, 11215–11220.
- 199 H.-i. Kim, D. Monllor-Satoca, W. Kim and W. Choi, *Energy Environ. Sci.*, 2015, **8**, 247–257.
- 200 Y. Park, S. H. Lee, S. O. Kang and W. Choi, *Chem. Commun.*, 2010, **46**, 2477–2479.
- 201 S. K. Choi, H. S. Yang, J. H. Kim and H. Park, *Appl. Catal., B*, 2012, **121–122**, 206–213.
- 202 V. H. Houlding and M. Gratzel, *J. Am. Chem. Soc.*, 1983, **105**, 5695–5696.
- 203 S. Ikeda, C. Abe, T. Torimoto and B. Ohtani, *J. Photochem. Photobiol. A*, 2003, **160**, 61–67.
- 204 G. Kim and W. Choi, *Appl. Catal., B*, 2010, **100**, 77–83.
- 205 S. Kim and W. Choi, *J. Phys. Chem. B*, 2005, **109**, 5143–5149.
- 206 J. M. Notestein, E. Iglesia and A. Katz, *Chem. Mater.*, 2007, **19**, 4998–5005.
- 207 Y. Park, N. J. Singh, K. S. Kim, T. Tachikawa, T. Majima and W. Choi, *Chem. – Eur. J.*, 2009, **15**, 10843–10850.
- 208 P. Persson, R. Bergstrom and S. Lunell, *J. Phys. Chem. B*, 2000, **104**, 10348–10351.
- 209 Y. S. Seo, C. Lee, K. H. Lee and K. B. Yoon, *Angew. Chem., Int. Ed.*, 2005, **44**, 910–913.
- 210 M. Yang, D. W. Thompson and G. J. Meyer, *Inorg. Chem.*, 2002, **41**, 1254–1262.
- 211 G. Zhang and W. Choi, *Chem. Commun.*, 2012, **48**, 10621–10623.
- 212 W. R. Duncan and O. V. Prezhdo, *Annu. Rev. Phys. Chem.*, 2007, **58**, 143–184.
- 213 E. Bae and W. Choi, *J. Phys. Chem. B*, 2006, **110**, 14792–14799.
- 214 E. Bae, W. Choi, J. W. Park, H. S. Shin, S. B. Kim and J. S. Lee, *J. Phys. Chem. B*, 2004, **108**, 14093–14101.
- 215 H. Park and W. Choi, *Langmuir*, 2006, **22**, 2906–2911.
- 216 H. Park, E. Bae, J. J. Lee, J. Park and W. Choi, *J. Phys. Chem. B*, 2006, **110**, 8740–8749.
- 217 W. Kim, T. Tachikawa, T. Majima, C. Li, H.-J. Kim and W. Choi, *Energy Environ. Sci.*, 2010, **3**, 1789–1795.
- 218 D. P. Arnold and J. Blok, *Coord. Chem. Rev.*, 2004, **248**, 299–319.
- 219 *Photochemistry of Polypyridine and Porphyrin Complexes*, ed. K. Kalyanasundaram, Academic Press, San Diego, 1992.
- 220 A. G. Agrios, K. A. Gray and E. Weitz, *Langmuir*, 2004, **20**, 5911–5917.
- 221 T. Tachikawa, S. Tojo, M. Fujitsuka and T. Majima, *J. Phys. Chem. B*, 2004, **108**, 5859–5866.
- 222 G. Kim, S.-H. Lee and W. Choi, *Appl. Catal., B*, 2015, **162**, 463–469.
- 223 Y. Cho, H. Kyung and W. Choi, *Appl. Catal., B*, 2004, **52**, 23–32.
- 224 Y. K. Kim, S. Lee, J. Ryu and H. Park, *Appl. Catal., B*, 2015, **163**, 584–590.
- 225 H. Wender, A. F. Feil, L. B. Diaz, C. S. Ribeiro, G. J. Machado, P. Migowski, D. E. Weibel, J. Dupont and S. R. Teixeira, *ACS Appl. Mater. Interfaces*, 2011, **3**, 1359–1365.
- 226 M. C. Wu, J. Hiltunen, A. Sapi, A. Avila, W. Larsson, H. C. Liao, M. Huuhtanen, G. Toth, A. Shchukarev, N. Laufer,



- A. Kukovecz, Z. Konya, J. P. Mikkola, R. Keiski, W. F. Su, Y. F. Chen, H. Jantunen, P. M. Ajayan, R. Vajtai and K. Kordas, *ACS Nano*, 2011, **5**, 5025–5030.
- 227 X. Y. Zhang, H. P. Li, X. L. Cui and Y. H. Lin, *J. Mater. Chem.*, 2010, **20**, 2801–2806.
- 228 B. Zielinska, E. Borowiak-Palen and R. J. Kalenczuk, *Int. J. Hydrogen Energy*, 2008, **33**, 1797–1802.
- 229 H. Park, A. Bak, A. Y. Ahn, J. Choi and M. R. Hoffmann, *J. Hazard. Mater.*, 2012, **211–212**, 47–54.
- 230 H. Park, C. D. Vecitis, W. Choi, O. Weres and M. R. Hoffmann, *J. Phys. Chem. C*, 2008, **112**, 885–889.
- 231 H. Park, C. D. Vecitis and M. R. Hoffmann, *J. Phys. Chem. A*, 2008, **112**, 7616–7626.
- 232 H. Park, C. D. Vecitis and M. R. Hoffmann, *J. Phys. Chem. C*, 2009, **113**, 7935–7945.
- 233 J. Kim, W. J. K. Choi, J. Choi, M. R. Hoffmann and H. Park, *Catal. Today*, 2013, **199**, 2–7.
- 234 S. Y. Yang, W. Choi and H. Park, *ACS Appl. Mater. Interfaces*, 2015, **7**, 1907–1914.
- 235 T. Sakata, in *Photocatalysis: Fundamentals and Applications*, ed. N. Serpone and E. Pelizzetti, John Wiley & Sons, New York, 1989.
- 236 E. Borgarello, J. Kiwi, E. Pelizzetti, M. Visca and M. Gratzel, *Nature*, 1981, **289**, 158–160.
- 237 H. Park and W. Choi, *Catal. Today*, 2005, **101**, 291–297.
- 238 J. Kim, Y. Park and H. Park, *Int. J. Photoenergy*, 2014, **2014**, 324859.
- 239 Y.-J. Cho, H.-i. Kim, S. Lee and W. Choi, *J. Catal.*, 2015, **330**, 387–395.
- 240 S. Bae, S. Kim, S. Lee and W. Choi, *Catal. Today*, 2014, **224**, 21–28.
- 241 M. Sadeghi, W. Liu, T. G. Zhang, P. Stavropoulos and B. Levy, *J. Phys. Chem.*, 1996, **100**, 19466–19474.
- 242 G. Khan, Y. K. Kim, S. K. Choi, D. S. Han, A. Abdel-Wahab and H. Park, *Bull. Korean Chem. Soc.*, 2013, **34**, 1137–1144.
- 243 J. Choi, H. Park and M. R. Hoffmann, *J. Phys. Chem. C*, 2010, **114**, 783–792.
- 244 J. N. Kondo, D. Nishioka, H. Yamazaki, J. Kubota, K. Domen and T. Tatsumi, *J. Phys. Chem. C*, 2010, **114**, 20107–20113.
- 245 M. Katayama, D. Yokoyama, Y. Maeda, Y. Ozaki, M. Tabata, Y. Matsumoto, A. Ishikawa, J. Kubota and K. Domen, *Mater. Sci. Eng., B*, 2010, **173**, 275–278.
- 246 G. L. Chiarello, E. Sellli and L. Forni, *Appl. Catal., B*, 2008, **84**, 332–339.
- 247 J. S. Jang, S. H. Choi, H. G. Kim and J. S. Lee, *J. Phys. Chem. C*, 2008, **112**, 17200–17205.
- 248 C.-W. Tsai, H. M. Chen, R.-S. Liu, K. Asakura and T.-S. Chan, *J. Phys. Chem. C*, 2011, **115**, 10180–10186.
- 249 M. Mrowetz and E. Sellli, *New J. Chem.*, 2006, **30**, 108–114.
- 250 J. Kim and W. Choi, *Energy Environ. Sci.*, 2010, **3**, 1042–1045.
- 251 Y. Cho, H. Park and W. Choi, *J. Photochem. Photobiol., A*, 2004, **165**, 43–50.
- 252 J. Ryu and W. Choi, *Environ. Sci. Technol.*, 2008, **42**, 294–300.

